



Invited Review Paper in Commemoration of Over 50 Years of Oxidation of Metals: Alumina Scale Adhesion Mechanisms: A Retrospective Assessment

James L. Smialek¹

Received: 9 August 2021 / Revised: 26 November 2021 / Accepted: 28 November 2021 /
Published online: 7 January 2022

© The Author(s), under exclusive licence to Springer Science+Business Media, LLC, part of Springer Nature 2022

Abstract

Key factors related to protective alumina scale adhesion are reviewed in an historical context. Critical experiments that solidified the framework of new understanding are highlighted. These include scanning and transmission electron microscopy (SEM/STEM), scanning and hot stage Auger, X-ray photoelectron spectroscopy, analytical electron microscopy and focused ion beam (FIB-STEM) analyses of reactive element (RE) segregation, photo-luminescence spectroscopy, creep tests of RE-doped Al_2O_3 , imaging secondary ion mass spectrometry, S-RE or Hf/Y co-doped alloys, desulfurization, and density functional theory models of doped interfaces. The popular mechanisms (pegging, growth stress, scale plasticity, vacancy sink, chemical bond) are each addressed by simple logic tests. In some instances, the opposite of what was initially proposed is actually the case, thus discounting that mechanism. In contrast, chemical bond explanations survive these tests and are discussed in more detail. Control of sulfur segregation is presented as both necessary and sufficient for scale adhesion. Reactive elements also segregate and strengthen the scale-metal interface, while, at the same time and more importantly, they prevent sulfur interfacial segregation and bond weakening. Kinetic effects (Al_2O_3 grain boundary diffusion) are of fundamental oxidative interest, but cannot account for first-order effects on adhesion. These precepts are consistent with historical and recent industrial successes, for example, RE-doped FeCrAl heater/structural alloys, Hf-doped Ni(Pt) Aluminide bond coats, and melt-desulfurized (0.1 ppmw S) Ni-base superalloys. Outstanding issues for which further investigation may prove insightful or advantageous are noted.

Graphical Abstract

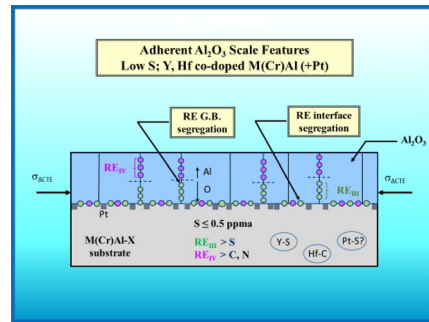
- Pegging, vacancy sink, scale plasticity, growth stress, graded seal theories refuted.

James L. Smialek: Retired.

Extended author information available on the last page of the article

- Chemical bond (segregation) mechanisms supported.
- Low S prevents segregation, interface voids, spallation.
- RE doping prevents S segregation; increases adhesion.
- RE_{III}(Y) dopants decrease Al outward, RE_{IV}(Hf) decrease O inward g.b. diffusion and growth.

- Pegging, vacancy sink, scale plasticity, growth stress, graded seal theories refuted.
- Chemical bond (segregation) mechanisms supported:
- Low S prevents segregation, interface voids, spallation.
- RE doping prevents S segregation; increases adhesion.
- RE_{III}(Y) dopants decrease Al outward, RE_{IV}(Hf) decrease O inward g.b. diffusion and growth.



Keywords Alumina scale adhesion · Sulfur segregation · Reactive elements · Ni-base superalloys

Abbreviations

TGA	Thermogravimetric analysis
SEM	Scanning electron microscopy
TEM	Transmission electron microscopy
EDS	Energy dispersive spectroscopy
AEM	Analytical electron microscopy
STEM	Scanning transmission electron microscopy
FIB-(STEM)	Focused ion beam (thinning)
SIMS	Secondary ion mass spectroscopy
ToF (SIMS)	Time-of-flight SIMS
SNMS	Secondary neutral (species) mass spectroscopy
PLS	Photoluminescence spectroscopy
AES	Auger electron spectroscopy
SAM	Scanning Auger microscopy
GDMS	Glow discharge mass spectroscopy
GDOES	Glow discharge optical emission spectroscopy
DTS	Desk top spallation
TBC	Thermal barrier coating
MIDS	Moisture-induced delayed spallation
MIHE	Moisture-induced hydrogen embrittlement
DFT	Density functional theory
DV- $X\alpha$	Discrete variation $X\alpha$ cluster function
VASP	Vienna ab initio simulation program

Introduction

Since the inception of This Journal in March 1969, one of the most popular, if not controversial, topics has been the mechanism of Al_2O_3 (and Cr_2O_3) scale adhesion. A handful of different, though related, theories have been proposed to explain the dramatic beneficial effects that ~ 0.1 wt% reactive element additions can make to scale adhesion and cyclic oxidation resistance. There is little dispute that reactive elements have this effect. The controversy arises from multiple secondary effects (“The Trees”) that may be causative, coincident, or somewhere in between. Indeed, RE doping may be sufficient, *but not necessary*, to produce scale adhesion. It is maintained that, if secondary effects can be dismissed in light of contradicting evidence, perhaps a more universal scheme (“The Forest”) can be embraced. If one unifying aspect is indispensable for adherence, regardless of various other complex features, it garners an overarching position as the most likely underlying *necessary* factor. More simply, the approach is to apply Occam’s Razor wherever possible and choose a single explanation rather than a collection of complex arguments, as suggested by Lees in 1987 [1]^(OM-100), (where^(OM-100) or^(OM-1000) citations refer to pivotal Oxidation of Metals references in this paper with over 100 or 1000 citations). This commentary will address various proposals from a historical standpoint, highlighting the significance of experimental and theoretical tools of that era, as well as critical experiments that helped eliminate some ambiguity. To some extent it will reiterate and embellish his subsequent treatise, regarding both alumina and chromia scales [2]. However, the focus of the present study will be on alumina scales.

More current assessments by Pint [3]^(OM-1000), now accepted in large part, refute prior speculative proposals and recognize multiple beneficial RE aspects as follows:

Inhibition of outward Al transport decreases the counter vacancy flux to the interface.

Segregation of RE ions to the interface decreases the interfacial energy and thereby increases the critical scale thickness sustained before spallation.

RE additions prevent the interfacial segregation of S which has a detrimental effect on void growth [and intrinsic interfacial toughness]. The observed outward flux of RE ions from the alloy into the scale results in RE ions segregated at the metal-scale interface [and grain boundaries].

Another motivation of the present paper is to highlight early historical contributions, ca. 1970–1990, sometimes limited by the technology of that day. Nevertheless, these are seen to set the stage for a resurgence of post-millennium studies, now enabled by more advanced techniques.

Background

First, we should step back and say that, for most oxidation studies, scale adhesion is most often and conveniently categorized by loss of surface scale (spalling), observed either microstructurally, by weight loss, or both. This may

result after cooling from isothermal or cyclic oxidation exposure and typically involves a large compressive stress on the scale due to thermal expansion mismatch with the underlying alloy. For example, the coefficient of thermal expansion for $\alpha\text{-Al}_2\text{O}_3$ is $\sim 9 \times 10^{-6}/^\circ\text{C}$, while those of the metal substrates oxidized are $\sim 15\text{--}18 \times 10^{-6}/^\circ\text{C}$, with exposure temperatures typically ranging from 1000° to 1200°C . Intrinsic “Adhesion” may also be addressed more directly by pull-off tests, scratch tests, frictional measurements, or computational oxide-metal bonding theoretical approaches. The direct experimental techniques are specialized and require that some scale must be retained after exposure. Microstructure and weight change remain the predominant observational measures.

This commentary will not provide an extensive literature review, normally entailing hundreds of relevant studies. Previous overviews [4–9] have been provided by Whittle [4], Hindam [5]^(OM-100), Smialek [6], King [7], Lang [8], and Stott [9]^(OM-100) from 1980 to 1995. Nor will it cover analogous RE effects for Cr_2O_3 scales having more complex kinetic and diffusional aspects. The latter do not apply nearly as strongly to Al_2O_3 scales, diminishing arguments based on growth direction and rates. Over time, the more protective Al_2O_3 scales commanded greater attention for higher temperature alloys.

More recently, special symposia and keynote reviews by Pint [10], Hou [11], and Naumenko et al. [12] have been dedicated to the subject. Additional contributions by Pint have provided perhaps the most extensive data set regarding reactive element gravimetric effects on oxidation, scale adhesion, and failure times, as compiled in his chapter in Shreir’s *Corrosion* [13]. Rather than providing a review, the present commentary provides a personal perspective adopted over decades of interest, aimed at critical elements of the phenomenon. Many of these elements originated by authors of historic note (e.g., Tien and Pettit [14], Golightly et al. [15]^(OM-100), Hindam and Whittle [5], Whittle and Stringer [4], Huntz et al. [16] etc.). Their contributions, noted and often personally discussed at the time of publication, helped evolve the present perspective.

We begin with early contributions of the founding editor, Prof. David Douglass on Y and Th reactive element effects on NiCrAl oxidation [17, 18]^(OM-100). Two studies identified only small changes in growth rate, controlled by inward grain boundary diffusion of oxygen along columnar grains. At low doping levels, adhesion was markedly improved, without pegs. However, detrimental spallation effects due to excessive amounts of RE (overdoping) were triggered at ThO_2 precipitates or yttrium aluminum garnet (YAG, see Glossary of acronyms) arising from the oxidation of YNi_9 . These particles were proposed as vacancy sinks to reduce back diffusion of Ni and Kirkendall void nucleation. In retrospect, many of the micro-voids shown were entrapped in the scale or were simply dimples within Al_2O_3 grains, and thus probably not operative for spallation.

Another early but, nevertheless, quite prophetic study directed toward scale adhesion mechanisms on NiCrAl(Y) and CoCrAl(Y) alloys, also used thermogravimetric (TGA) and scanning electron microscopy (SEM, just maturing for oxidation studies ca. 1970) [19]. Giggins and Pettit [19] concluded a number of salient points: again, no effect of Y on growth rate, sufficient scale plasticity and deformation on undoped alloys, no graded seal, voidage was unnecessary for spallation, and no spallation of

Y-doped scales subjected to large external stresses (bending). These early observations provided a significant narrowing of viable mechanisms and have been reinforced over the years.

Another motivating, illuminating, and innovative study was presented by Smeggil at the 1983, ECS High Temperature Chemistry Symposium, Cincinnati, OH [20]. Here, strong sulfur surface segregation on undoped NiCrAl (from just a few ppmw in the bulk) was reduced by Y-doping, as first revealed by high temperature Auger spectroscopy. This implicated detrimental sulfur impurity segregation effects on chemical bonding. These findings were incorporated in the broader *dynamic segregation* model [3] ^(OM-1000). Here RE segregation to the oxide-metal interface, grain boundaries in the scale, and effects on ion diffusion, scale growth, sulfur segregation, and void growth were outlined. In large part these proposals stand with few reservations, and, along with early works by Smeggil, Lees, Smialek, Grabke, Hou, Meier, Pettit et al., provide a framework for ongoing critical examinations of alumina scale adhesion mechanisms.

In the present commentary, for the sake of simplicity, we can shorthand the familiar theories addressed above according to the nomenclature: 1. Pegging, 2. Scale Plasticity, 3. Growth Stress, 4. Vacancy Sink, and 5. Chemical Bonding. This latter category will include a variety of RE, S, Pt, H₂O, and DFT considerations.

As the field has widened its scope, various terminologies for the term “adhesion” are implied. Typically, alumina scale adhesion is illustrated through cyclic oxidation sample weight change data. Weight decreases from scale spallation can overtake the initial increase from scale growth, leading to negative weight change and eventually non-protective, complex scales. Spallation is promoted by larger compressive stresses (higher temperature cycling or thermal expansion mismatch). The interface toughness may be weakened by defects (porosity, voids, wrinkling or convolutions) as well as by impurity segregation, all producing increased spallation. The actual scale-metal “adhesion” strength has occasionally been measured by epoxied stub, tensile pull tests or by in-situ micro-stylus scratch tests. Model studies that address *bulk* Al₂O₃–metal “adhesion” bond strengths and fracture toughness as a function of impurity segregation are supportive, but not addressed here. Finally, ab-initio calculations address the theoretical bonding of oxide atoms to metal atoms across a low index, coherent interface, yielding the work or energy of separation or “adhesion.” The term “adhesion” can therefore imply various quantities depending on the nature of the specific study.

Proposed Adhesion Mechanisms and Processes

Pegging

Oxide intrusions or pegging was the earliest observation and proposed mechanism for scale adhesion as previously reviewed, e.g., in ref. 4. RE additions often resulted in irregular scale-metal interfaces, with distinctive fingers of oxide keyed into the metal. The RE, able to oxidize at a lower p_{O_2} than Al, is thought to partially oxidize near the surface and provide fast diffusion paths for Al₂O₃ to grow, but in a

non-planar fashion. The additional surface area and mechanical locking were suggested to provide increased attachments that provided the dramatic improvements in scale adhesion. The evidence was typically provided by cross-section optical/SEM microscopy and SEM of detached scale undersides. At high dopant levels, the extent of oxide intrusions can be large and contribute to higher weight gains. However, adhesion can be provided at lower dopant levels where little or no pegs are observed. In the case of NiCrAlY, the improved bond was also attributed to ‘micro-pegs [19].’ While intuitively persuasive, mechanical stress/toughness analyses were generally not provided. That is, how much might the mechanical adhesion strength be increased with certain distributions of oxide intrusions? Relevant considerations might have been increased surface area and frictional resistance, interfacial shear stress, fracture toughness and cracking of small intrusions.

Examples of adherent scales without pegs would be exclusionary to a mechanism based on the existence of pegs. Indeed, occasions abound where pegs were not necessary for adherent alumina scales. For instance, a high purity FeCrAlY alloy was oxidized at 1200 °C for 100, 500, and 2000 h with no spallation noted [21]. Quality cross-sectional SEM, including an iconic color SEM-EBSD image of columnar grains after 2000 h at 1200 °C, show an essentially flat, featureless interface. Similarly, flat and structurally clean interfaces have been documented by FIB-STEM. The aesthetic scale microstructure provided by K. Unocic, ORNL, shown in Fig. 1, was obtained from highly oxidation resistant Plansee PM 2000 (dispersion strengthened Fe–20Cr–5.5Al–0.5Ti–0.5Y₂O₃ wt%) after 8 h oxidation at 1100 °C in air–10% H₂O [22]. Columnar grains are prominent in the scale, and dislocations are present in the underlying alloy. No intrusions are evident. Furthermore, clean and nearly featureless interfaces have been shown after 1200 °C, 200 h oxidation of Kanthal APM (Fe–20Cr–5.5Al–0.03Ti wt% – 2vol% ZrO₂–Al₂O₃) and after 120 h oxidation of MA956 (Fe–20Cr–4Al–0.35Ti wt% – 3vol% Y₂O₃–Al₂O₃) by Tolpygo

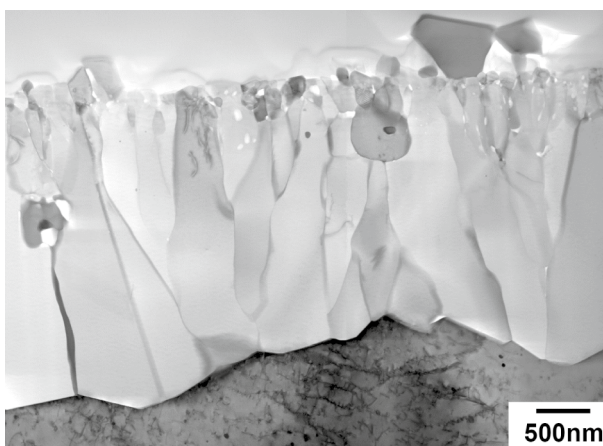


Fig. 1 FIB-STEM bright field high magnification cross-section and interface of adherent Al₂O₃ scale formed on Plansee PM 2000 FeCrAlTi–Y₂O₃ after 8 h oxidation in air–10% H₂O at 1100 °C. [Courtesy of K. Unocic, ORNL, 2017] [22]

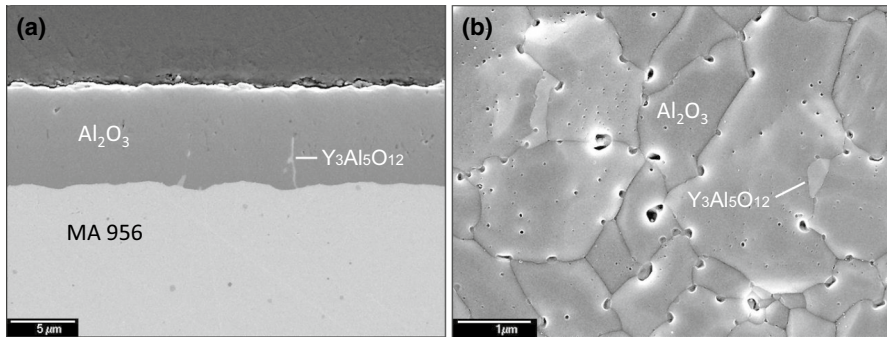


Fig. 2 SEM-SE images of ‘clean’ oxide-metal interface for MA 956 FeCrAlTi–Y₂O₃ oxidized at 1200 °C for 120 h: **a** polished cross-section; **b** underside of removed scale. (Courtesy of V. Tolpygo, presented at HTCMP-7, les Embiez, 2008)

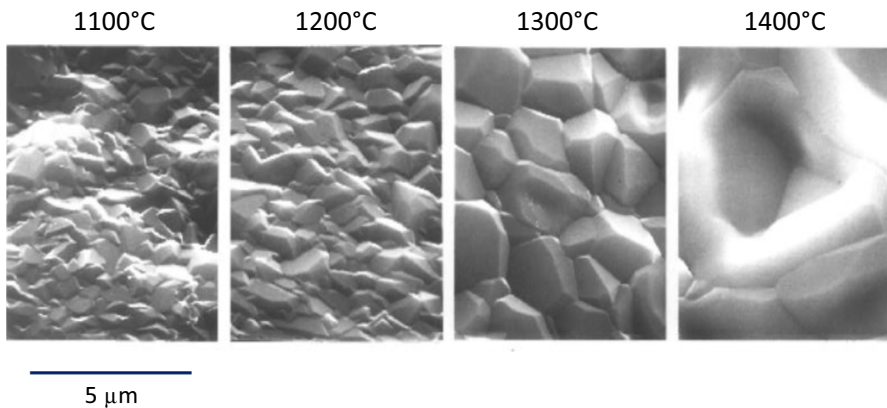


Fig. 3 SEM-SE images of ‘clean’ scale underside for Hoskins 875 (Fe–22.5Cr–5.5Al–0.5Si–0.2Zr) oxidized for 100 h at 1100 °C, 1200 °C, 1300 °C, and 1400 °C and delaminated by epoxied tensile stub [24]

[23]. This was shown both by cross-section and scale undersides, the latter revealed by chemically etching away the substrate, Fig. 2.

At NASA Glenn, the rolled strip heater alloy Hoskins 875 (Fe–22.5Cr–5.5Al–0.5Si–0.2Zr wt%) had been employed as an accessible, reproducible, alumina-forming alloy standard of comparison. The scale underside (Fig. 3) was revealed using an adhesion jig (tensile delamination via stubs joined to the oxide and metal substrate by epoxy) [24]. Rough estimates of delamination stress (if successfully delaminated) was ~70 MPa (10 ksi) or about the strength of the epoxy. No widespread peg features were observed. Yet, spallation after substantial isothermal or cyclic thermal exposures was rare or limited to only a few small areas. Surface views of the scale showed monoclinic ZrO₂ precipitates at the higher temperatures, Fig. 4, indicating Zr reactive element diffusion through the scale. The weight change curves for the corresponding interrupted exposures

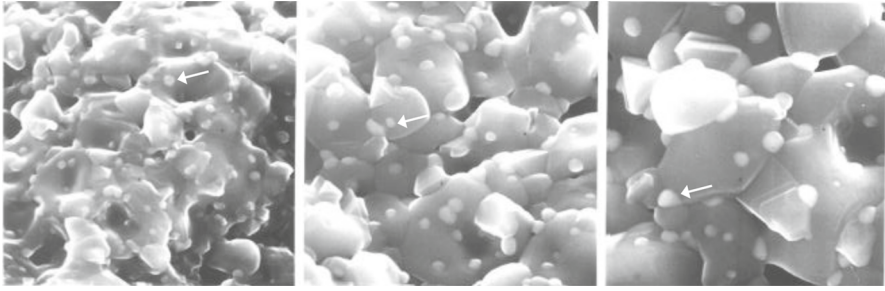


Fig. 4 SEM-SE images of ZrO_2 (m) surface precipitates formed above Al_2O_3 scale on Hoskins 875 FeCrAl(Si,Zr) after 1, 10, 100 h oxidation at 1400 °C

at 1100°–1400 °C indicate continuous protection without losses due to spallation [25]. These and further kinetic considerations regarding grain boundary transport were also presented. Further extremes in cooling temperature (to – 200 °C) had been examined in typical 1200 °C, 1-h cyclic tests, Fig. 5 [26]. Again, the response revealed no weight loss for this alloy, even with the additional thermal cycling range and associated expansion mismatch stress.

Thus, oxidation resistant FeCrAl-X alloys are well known. Other examples of adherent scales without pegs are available. For example, low sulfur (0.4 ppmw) single crystal superalloy René N5 was oxidized at 1100 °C for 100 h and exhibited an extremely clean, flat interface between the Al_2O_3 inner scale and the alloy [27]. More will be stated about oxidation resistant single crystal superalloys later.

At this juncture, it can be concluded that:

Pegs are not necessary for adhesion

(see the “[Appendix](#)” for logic tests of pegging and other mechanisms)

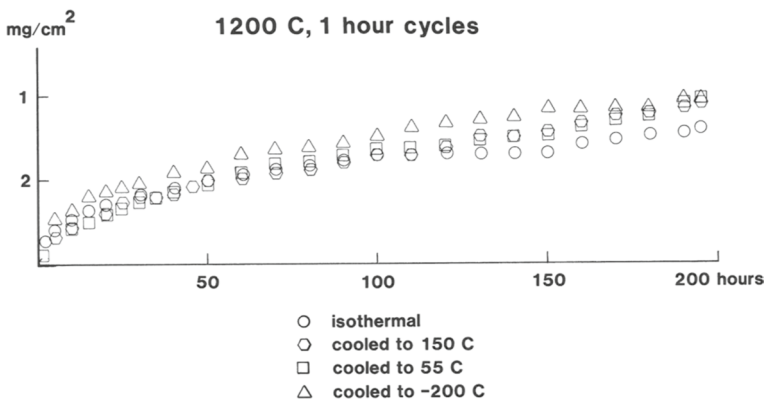


Fig. 5 Cyclic (1-h heating) weight change data for Hoskins 875 FeCrAl(Si,Zr) oxidized at 1200 °C for 200 h. Adherent behavior, equivalent to isothermal, for cooling to 150 °C, 55 °C, or – 150 °C [26]

Scale Plasticity

Scale plasticity adhesion mechanisms typically cite a finer grain scale developed on RE-doped alloys compared to that formed on undoped alloys. The argument entails a stress-relief process in a scale that has more grain boundary area available for easy grain boundary sliding or diffusional creep at high temperature. This could partially relieve compressive growth stress and subsequent total stress in the scale after cooling. It is argued that adhesion is therefore maintained because the total strain energy available for scale delamination is reduced. The rationale assumed some participation of RE (segregation) in the scale microstructure. However, the precept, when proposed, did not benefit from atomistic or chemical grain boundary imaging of scales now more available with FIB-STEM.

In the following, it is maintained that reactive elements segregate to the alumina scale grain boundaries. This phenomenon actually enhances strength and reduces scale plasticity. Initially, (ca. 1985) surface segregation in high temperature Auger spectroscopy systems by Smeggil [28], Luthra [29]^(OM 100), and Smialek et al. [6] indicated the segregation potential of reactive elements. ZrO₂ grain boundary precipitates had been seen at the gas surface of Hoskins 875 FeCrAlSiZr, Fig. 2 [24], implying Zr diffusion occurred through the scale, presumably along short-circuit grain boundary paths. STEM analyses have since identified RE grain boundary segregation conclusively. Y and Ti were first observed (1987) at the scale-metal interface and at Al₂O₃ grain boundaries in oxidized MA 956 by Przybylski et al. [30]. Similarly, Y and Zr segregation were observed at the same locations for oxidized Kanthal APM FeCrAl – ZrO₂ [31]. Confirmation of RE segregation along with documentation of sulfur interfacial segregation was provided by similar cross-section STEM analyses [32]^(OM-100). It is now well established that RE dopants segregate to the oxidizing interface and become incorporated in the Al₂O₃ scale grain boundaries. For reference, *dynamic segregation* [3]^(OM-1000) became part of the RE-effect lexicon, reinforced by both prior and subsequent studies. Here Y, Zr, and Ti were clearly demonstrated as concentrating in the grain boundaries and gas surfaces of growing Al₂O₃ scales on oxidation-resistant, alumina-forming Fe–20Cr–5Al–0.3Ti–Y₂O₃ MA 956 and NiAl–0.2Zr, wt%. With the development of FIB-STEM techniques, the elemental mapping of segregated interfaces has become more prevalent, e.g., Hf segregation at Al₂O₃ boundaries formed on a commercial MCrAl–Y,Hf,Si coating (PWA 286) [33]. Similarly, Hf, Zr, Y, and Ta grain boundary segregation was vividly illustrated by STEM-EDS elemental maps for René N5 oxidized for 100 h at 1100°C [27]. And Ti, Y grain boundary segregation was shown for ODS FeCrAlTi–Y₂O₃ PM 2000 after 8 h at 1100 °C oxidation in 50H₂O–50(CO₂–0.15O₂), Fig. 6, courtesy K. Unocic [22].

One significant and typical effect of doped Al₂O₃ grain boundaries is sintering and strengthening. Briefly, it is well known that reactive element dopants segregate to grain boundaries in bulk alumina and affect grain growth, sintering, and creep [34] Generally, grain boundary diffusivity and sliding are key factors. It is reported that creep rates are reduced 2–3 orders of magnitude by Nd, Zr co-doping because of high observed segregation fractions [35]. Given that α -Al₂O₃ scales formed on doped alloys consistently show RE grain boundary segregation at appreciable levels,

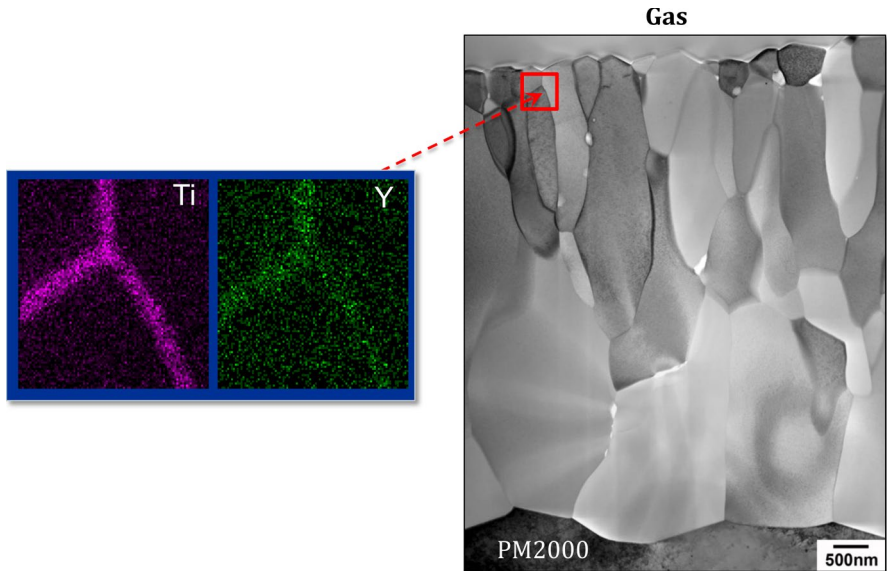


Fig. 6 FIB-STEM bright field high magnification cross-section and EDS maps showing Ti, Y grain boundary segregation in adherent Al_2O_3 scale formed on Plansee PM 2000 FeCrAlTi– Y_2O_3 after 8 h oxidation at 1100 °C in (50 CO_2 –50 H_2O)—750 ppm O_2 [Courtesy of K. Unocic, ORNL, 2017] [22]

it is reasonable to expect that creep strengths of the scales have been increased accordingly. Thus, an adhesion mechanism based on increased scale plasticity would be in opposition to fundamental properties measured on bulk alumina. Rather, it would be expected that doped scales maintain a higher strength at temperature and do not preferentially reduce stress by scale plasticity. (This phenomenology is also directly pertinent to the next hypothesis on growth stress).

In summary, it is concluded: *Enhanced scale plasticity would be expected for undoped $\alpha\text{-Al}_2\text{O}_3$ scales, i.e., associated with non-adherent behavior. Doped scales would be stronger and less plastic, but are associated with adherent behavior.*

Growth Stress

The flat, planar geometry of scales formed on doped alloys compared to wrinkled, convoluted scales on undoped alloys has also led to the growth stress hypothesis. Namely, reactive elements alter transport in the oxide so as to reduce (Al outward) scale growth that can generate excess volume within the oxide and cause compressive (growth) stress. Equiaxed or duplex scales formed on undoped alloys are cited as evidence for some outward Al diffusion and growth within the oxide, while columnar scales, perhaps with finer grain size, formed on RE-doped alloys indicate primarily O inward diffusion, enabling stress-free growth at the scale metal interface [15]^(OM-100). The elegance and self-consistent correlations of microstructure,

deformation, transport, voids, and adhesion allowed this mechanism to gain traction among the oxidation community.

A consolidated inward growth direction has been confirmed in many subsequent studies of RE doped systems. Dopant effects on transport properties in bulk Al_2O_3 and Al_2O_3 scales is another extensive subject unto itself. However, the following direct observation, espoused in their detailed, seminal work, leads to this unequivocal statement negating the growth stress mechanism: “The presence of the reactive element, yttrium, suppresses wrinkling and restricts lateral growth, but it does **not** decrease the stress in the oxide [36].” ... “The alumina scales formed on [FeCrAl] alloys containing yttrium are under a *larger* compressive stress than those formed on yttrium-free alloys.... Thus, one possible role for yttrium is to decrease the alumina creep rate to the level where the scale cannot deform by wrinkling [37] ^(OM-100)”. This conclusion was obtained from extensive direct measurements of stress in the scales by photoluminescence optical spectroscopy (PLS or piezospectroscopy), pioneered by Clarke, Lipkin, Tolpygo, and colleagues [36–38] ^(OM-100) [39, 40], combined with plastic strains measured in the alloy. A subsequent PLS study measured stress in the alumina scales as a function of substrate/scale thickness ratio, (H), for three thicknesses of FeCrAl(\pm Y) oxidized for three times at 1200°C [41]. The growth stress, obtained from the difference between the measured residual stress and that projected from thermal expansion mismatch stress, was found to saturate equally for both doped and undoped alloys near $H = 150$. Relaxation levels were also equivalent, though others observed faster relaxation for the undoped alloy. Growth stresses relaxed completely above 850 °C more rapidly as temperatures increased and for thin samples, before saturation when $H < 100$ –200, similar to Tolpygo. They concluded: “No significant differences in the growth stresses, total residual stresses, or stress relaxation during thermal cycling were observed between the oxides formed on the Y-doped and undoped FeCrAl samples [41].”

In PLS, frequency shifts in the Cr^{3+} R-line arise from internal stress in the corundum lattice, but is measured at room temperature on cooled samples. Residual compressive stresses after cooling were as high as -6 GPa for scales developed on FeCrAlY. Furthermore, compressive growth stresses of -1 GPa at temperature were typically deduced. Thus, it is not possible to argue that scales on doped alloys are adherent because they are under less stress than their undoped counterparts. A consolidated compilation of related growth stress observations from Tolpygo [40] ^(OM 100), Mennicke [41], and Meier (*) [42, 43], is presented in Table 1. Here, adherent scales are found for doped or low S FeCrAl alloys, regardless of growth stress or alloy elongation, i.e., high growth stresses may exist for adherent scales. Complete stress relaxation may occur in adherent and non-adherent systems, while adherence may be retained for low sulfur or doped FeCrAl samples showing substantial elongations. Thin samples can be expected to exhibit exaggerated elongation from scale CTE mismatch stresses, but sample thickness does not control adhesion unequivocally. A number of the exposure and sample details become complex regarding cooling rates, substrate thickness, crystallographic orientation, and alloy properties. Nevertheless, adhesion was most strongly correlated with *RE doping or low sulfur alloys—not geometry, stress in the scale, relaxation, or alloy deformation.*

Table 1 Compilation of FeCrAl results for growth stress, relaxation, and deformation as related to dopant, sulfur content, and adhesion

Alloy	Condition	PLS		Deformation		Adhesion
		Growth σ	Relaxation	Scale	Substrate	
FeCrAl	Undoped	- 1.25 GPa	0.0 GPa	High	Moderate	Poor
FeCrAl	- thin	Reduced	Increased	Reduced	Increased	Poor
FeCrAlY	Doped	- 1.25 GPa	0.0 GPa	Low	+2%	Good
FeCrAlY	- thin	Reduced	Increased	Low	Increased	Good
FeCrAl*	Undoped			Wrinkled	-0.4%	Poor
FeCrAl*	Low S			Planar	+0.7%	Good
FeCrAl*	Low S, thin		Planar	g.b. cusps	Good	
FeCrAlTi*	Doped			Planar	+0.9%	Good
FeCrAlHf*	Doped			Planar; intrusions	Low	Good
FeCrAlY*	Doped			Planar	-0.1%	Good

PLS measurements of isothermally grown alumina scales. Undoped FeCrAl scales formed at 1000 °C, 1200 °C; doped FeCrAlY scales formed at 1000°–1300 °C [36, 37, 41]. Also, *Cyclic oxidation: weight change and microstructure at 1100 °C (45-min. cycle) and substrate elongation at 1200 °C (24-h cycle) [42, 43]

Y-doping effects on the fracture toughness of the scale-metal interface was strongly implicated.

This conclusion was foretold in an early 1975 study that stated: "...bending oxidized CoCrAlY at room temperature did not produce widespread spalling. Therefore, models based on reduced stress levels (scale plasticity, stress relief, or reduced growth stress) are unacceptable. Rather, some source of improved bonding must apply [19]." Accordingly, most of the present paper addresses improved bonding.

Also, along the lines of growth stress, it is pertinent that FeCrAl (Ti, Hf, Y) alloys present interesting results for long term cyclic oxidation testing at 1100 °C, Table 1. The Ti-doped alloy presented surface deformations, but no interface voids or spallation after ~1300 (hot) hours of oxidation. The Hf-doped FeCrAl also remained adherent, exhibited oxide intrusions, but the interface remained planar. Lastly, the Y-doped FeCrAl remained adherent and presented a uniformly flat surface with no oxide intrusions. By comparison, an undoped, hydrogen-annealed, desulfurized sample (~0.1 ppmw S) remained quite adherent and essentially planar for nearly 800 h, with no oxide intrusions or voids. It did present some local contortions that followed deformation with the alloy after 1300 h of cyclic oxidation. The undoped, unannealed FeCrAl alloy (25 ppmw S) showed rumpling, voids, spallation, and breakaway after just 100 h. Here low sulfur FeCrAl therefore presented a *sufficient* criterion for adhesion and void prevention, even withstanding deformation of the alloy. RE doping also resulted in adhesion, with or without alloy deformation. It was shown that measurable elongations occurred for three FeCrAl alloys having adherent scales: undoped low sulfur, Hf- or Ti-doped. Here, the Y-doped FeCrAl did not elongate, whereas it did for a similar alloy studied by Tolpygo and Clarke [40] (OM-100). Thus, a one-to-one correlation of scale adhesion, deformation, stress relief,

and residual stress simply did not exist. Alloy mechanical properties are seen to be a factor on interface morphology and deformation, and perhaps long-term breakaway failure of adherent systems, but not necessarily affecting first order effects on interfacial adhesion. (The effectiveness of Ti alone in FeCrAl and its presence in a number of co-doped commercial FeCrAl alloys reoccurs as an unresolved feature of interest in future sections).

RE effects on bulk Al_2O_3 are equally dramatic. Harmer et al., have shown that Y, La, and Nd doping of polycrystalline Al_2O_3 (1–2 μm grain size) produced a two order of magnitude reduction in creep rate @ 50 MPa at 1200 °C. Nd/Zr co-doping produced an even larger reduction. Also, Zr, Hf doping produced a $15\times$ reduction in creep rate [35, 44–46]. Based on 12 dopant variations, Yasuda et al. [47] report a slight *increase* in 1250 °C creep rate @ 50 MPa only for Ti-doped Al_2O_3 (1 μm grain size), with progressive decreases in creep rate for Mg, Sr, Zr, Y, and a $400\times$ decrease for Y/Zr co-doped Al_2O_3 . While atomic size and fitting effects on grain boundary diffusion had been argued for reduced Coble creep, the latter study found no correlation with dopant atomic radius. They related singly and co-doped creep rates to the effective net charge on the oxygen ion, as modeled by the DV- $X\alpha$ (discrete variation $X\alpha$) cluster model method: “A first-principle molecular orbital calculation ...revealed that the value of NC [net charge] in O correlates with the creep rate in ...co-doped Al_2O_3 . The (greater) creep resistance ...is likely to be determined by (higher) ionicity of oxygen anion at the grain boundaries with dopant ...segregation.” Given that the scale grain sizes are generally 0.1–5 μm at most, and growth stresses of 1 GPa have been measured, it is not unreasonable to expect plastic deformation (creep) of undoped (and weaker Ti-doped) scales at 1100 °C and above. Other RE-doped scales are substantially stronger and able to sustain larger residual stresses without buckling. This contradicts growth stress precepts claiming that buckled scales imply higher stress. Ab initio, creep, transport, and cyclic oxidation studies raise questions about the role and effectiveness of RE co-doping for performance. Correlations vs cause and effect are of interest, but remain unresolved.

Returning to alumina scales on FeCrAl alloys, Y-doping prevented rumpling, but there may still be some growth within or above the oxide. Normally protective scales on doped alloys are considered to grow primarily by inward oxygen diffusion (with columnar grains), whereas outward aluminum diffusion for scales grown on undoped alloys allows growth within (or above) the scale (and equiaxed grains). These elements have been graphically illustrated via repolishing and re-oxidation of an intermediate scale or taper (wedge) section, where outward growth of new oxide, i.e., grain boundary ridges, were observed above pre-existing grain boundaries [48, 49] ^(OM-100). The outer layer of new growth was identified by the equiaxed morphology (as presented in 1976 by Golightly, Stott, and Wood for scale believed to grow with Al outward diffusion on undoped FeCrAl) [15] ^(OM-100). The degree of scale formed at 1200 °C by outward diffusion of Al was indeed measured as ~15% for Incoloy MA 956 FeCrAlY-Y₂O₃ and ~50% for Kanthal A-1 FeCrAlZr [49] ^(OM-100). It can also be seen that the outward growth does not necessarily indicate growth within the oxide, but rather on top of the oxide. As these new fine grain scales expand laterally, they encompass more of the outer surface area of the scale, and eventually coalesce, concealing the ridge morphology. Further outer layer growth can nucleate new fine

grains and promulgate the process. In retrospect, it is completely reminiscent of the distinctive oxide ridges formed over Al_2O_3 scales on $\beta\text{-NiAl}$ due to the $\theta\text{-}\alpha$ transition, discussed as a contribution of outward Al diffusion [50, 51]^(OM-100). Here, ridges and dimpled grains at the gas surface were also discussed for Al_2O_3 scales formed on Pt_2Al [52]^(OM-100) and Hoskins 875 FeCrAlZr [51]^(OM-100).

RE effects on grain boundary diffusion in Al_2O_3 are thus intrinsic to all the above considerations, but do not alter the basic conclusion that adherent scales can sustain large growth stresses. There is general agreement that RE doping reduces outward Al grain boundary diffusivity and transport in scales. The degree to which this happens may be fundamentally linked to the specific dopant and alloy. Typically, the O^{18} isotope is used as a radioactive tracer to monitor the growth direction by profiling after a double or two-stage $\text{O}^{16} + \text{O}^{18}$ oxidation treatment. Techniques have varied, starting in 1983 with $p\text{-}\alpha$ proton activation (nuclear reaction analysis), then numerous SIMS sputter profiling or imaging SIMS, and most recently ToF-SIMS [53, 54]^(OM-100), [55]. Dopant effects on transport in Al_2O_3 scales remain an important feature of oxidation, but do not always appear to directly figure in the main mechanisms controlling interfacial adhesion.

Comparing again to transport in bulk Al_2O_3 , a unique (oxygen permeability) technique has been perfected by Kitaoka et al. to examine grain boundary transport across polycrystalline Al_2O_3 wafers subjected to an oxygen potential gradient as it might relate to a growing scale [56–58]. Dopant effects were also studied. Briefly, it was concluded that Hf-doping reduced by $2\times$ the grain boundary diffusion product, $\delta D_{gb,Al}$ for Al at the high p_{O_2} side (as $\propto p_{\text{O}_2}^{3/16}$), with no effect on the low p_{O_2} side. Conversely, Lu or Y doping reduced $\delta D_{gb,O}$ by $3\times$ at the low p_{O_2} side (as $\propto p_{\text{O}_2}^{-1/6}$), with no effect on the high p_{O_2} side [56–58]. Co-doping may produce complex results depending on dopant location. For example, for a layered 2-wafer structure, the Lu doped wafer was only effective on the low p_{O_2} side (oxygen diffusivity), while the Hf-doped wafer was only effective on the high p_{O_2} side (aluminum diffusivity). Other co-doping issues will be addressed in subsequent sections.

While these bulk Al_2O_3 studies are illuminating and compelling regarding fundamentals of dopant effects, the trends are not always consistent with some of the observed Y, Hf, Zr effects on scale growth. In general, it is believed that most RE dopants reduce Al transport, and sometimes total scale growth, compared to an undoped alloy. But, for example, it was shown that Y_2O_3 (MA 956) doping produced somewhat greater inward oxygen growth than Zr-doping (Kanthal A-1), with less outward aluminum growth, (both alloys co-doped with Ti < 0.5 wt%) [49]^(OM-100). Furthermore, Ti- Y_2O_3 co-doped FeCrAl- was shown (by ^{18}O SNMS and SEM-EBSD) to produce more outward Al growth and external equiaxed grains on the outer scale (compared to total O inward columnar growth without Ti). It did so without significantly affecting total scale thickness with bilayers of doped Ti- or Y-rich grain boundaries [59]. Indeed, the transport mechanisms in doped bulk Al_2O_3 or Al_2O_3 scales warrant a full review unto themselves and are well beyond the scope of this commentary [60].

While specific transport mechanisms are crucial to detailed growth attributes and overall oxidation performance, they do not appear to explain the less-complicated, *binary* effect of dopants solely on adhesion. Pint, referring to his broad database of

RE-doped alumina-forming alloys concluded: “For determining (cyclic oxidation) lifetime, the RE effect on scale *adhesion* appears to be much more important than the effect on scale *growth rate*. Thus, reducing the scale growth rate will not necessarily result in an improvement in alloy lifetime [10].” Reduced kinetics for doped scales may, however, result in less stored (CTE mismatch) strain energy that is proportional to scale thickness. At most, the parabolic oxidation rate k_p of undoped scales may be 2–10× as great as those for doped scales. Yet they are likely to have failed early anyway, regardless of thickness, because of a dramatically weaker interface. The slowest growing doped scales might have longer lives than other doped scales with higher k_p , but not by the same degree compared to undoped alloys. Accordingly, the RE effect of reduced kinetics on Al_2O_3 scale spallation is not covered in great detail here.

Recapping with the logic test for Growth Stress:

High growth stress is not the root cause of spallation. Decreased growth stress is not necessary to produce adhesion.

Lastly, another stress aspect raised, but not demonstrated, in many early investigations has been that of a ‘graded seal’ to alleviate high interface stresses and prevent spallation. As explained by Giggins and Pettit [19], “The graded seal mechanism is based on a layer of oxide developed between the Al_2O_3 and the alloy which possess thermal expansion coefficients that gradually changeIn the present studies no such continuous layer has been observed.” This is consistent with all subsequent STEM observations of clean, phase-pure, and abrupt oxide-metal interfaces discussed previously. In summary:

No interfacial scale phase is observed for adherent scales; a graded seal is not necessary for adhesion.

Vacancy Sink

Most studies have observed voids at the oxide-metal interface for undoped alloys, in contrast to no voids for doped alloys. Internal RE oxides or complexes were proposed to serve as vacancy sinks and prevent void formation stemming from substantial outward Al growth and Al vacancy injection. Understandably, scale adhesion would be reduced by some factor proportional to the reduction in surface area of contact. Whether void prevention is sufficient to always enable scale adhesion is a reasonable question. Conversely, scales were observed to spall from undoped alloys having, in special cases, no interface voids [19]. The surface condition (electropolished) or long (isothermal) oxidation treatments may eliminate or maximize void production, respectively, without fundamentally changing the poor scale adhesion observed for undoped systems. Conversely, it has been shown that appreciable outward Al diffusion and outward scale growth can occur for RE-doped FeCrAl as well, without any interfacial voids or spallation [48, 49]^(OM-100). Thus, growth direction is not always uniquely correlated with interface voids and scale adhesion.

Another relevant feature of vacancy sinks would be the prevention of voids via oxide dispersions in the ODS substrate. However, other RE effects must be separated

from this proposal by using, say, Al_2O_3 dispersoids rather than RE ODS particles. Here, only a few studies [14] indicate that Al_2O_3 dispersoids may produce scale adhesion on their own, while others fail to confirm that effect [13]. This also casts doubt about the vacancy sink argument. This topic will resurface in the subsequent section regarding sulfur effects on interfacial void production.

Overall, it is concluded that:

Voids are not necessary for spallation. Outward growth is not sufficient to produce voids. Vacancy sinks are neither sufficient or necessary for adhesion.

Chemical Bonding

This tenuous state promoted continued discussions of, perhaps, misleading phenomena (e.g., voids vs wrinkled scales vs oxide intrusions vs dispersed oxides vs equiaxed/outward growing or columnar/ inward growing scales). Given disproven mechanisms above, a singular underlying overriding mechanism did not emerge.

Sulfur Effects, First Observations and Confirmations

We now address scale adhesion mechanisms based on chemical bonding. Here the alleged primary RE role is to prevent sulfur segregation at the oxide-metal interface. Sulfur is a well-known grain boundary segregant and embrittling agent in transition metals. Reactive elements are chemically active with sulfur, as they are to oxygen, with known thermodynamic correlations. Consequently, it was proposed that reactive elements retard sulfur segregation by reducing its thermodynamic activity globally in the lattice, if not also forming an actual RE-S compound. This allows the intrinsic clean interfacial bond strength to be maintained in typical high temperature (cyclic) oxidation exposures. Ultimately, adherent scales were produced *without* RE-dopants—by simply removing sulfur. It is believed that this is the only alternative means of producing adhesion other than by adding RE and warrants the exposition below.

Attention to sulfur effects during oxidation began in the mid-1980s with early revelations, by Smeggil and co-workers, that sulfur prominently segregated (over 20 at.% at the free metal surface) for NiCrAl having about 50 ppmw indigenous sulfur impurity [61]. The key experimental technique was hot stage Auger spectroscopy performed at 800°–1000 °C. In contrast, Y-doped NiCrAl exhibited only ~5–10 at.% sulfur segregation. Furthermore, serious scale spallation persisted with Y additions when provided only as Y_2S_3 , while more adherent behavior was restored by Y doping in addition to Y_2S_3 . This paper also identified S interfacial segregation and indigenous Y-S particles using microprobe and SEM, though at only 1 μm resolution.

Similar sulfur surface segregation and prevention by reactive elements were observed in a number of subsequent studies, and, ironically, by presenters in the same ECS meeting, Luthra and Briant [29] ^(OM-100). A similar treatise discussed chemical bond considerations [6], suggesting: "... agreement is lacking as to which mechanism is the most fundamental to adhesion mainly because exceptions have been found for each proposal." Again, hot stage Auger also found strong sulfur

surface segregation near 750 °C for undoped Ni–15Cr–13Al, but little or no sulfur for 0.5 wt% Y or Zr-doped NiCrAl, all having about 10 ppmw S [6]. This correlated with 1100 °C, 1-h cyclic oxidation spallation resistance, with 500 h weight changes of -13 mg/cm^2 , -1 mg/cm^2 , and $+3 \text{ mg/cm}^2$ for undoped, Y-doped, and Zr-doped alloys, respectively. It was also of interest that the Y- or Zr-doped alloys exhibited strong Y or Zr segregation, respectively. Bulk Al_2O_3 work of adhesion or frictional shear force correlations with the free energy of formation of oxides were raised as circumstantial evidence for RE bond enhancement [6]. Lastly, the enthalpy of formation of 40 metal sulfides and oxides were correlated, with sulfides tracking and averaging about $\frac{1}{2}$ that of the corresponding oxides, depending on the column in the periodic table. Sc, Y, Zr, La, Hf, Ce, and Th sulfides and oxides topped the enthalpy list, as do their free energies of formation [62–64]. Thus, the most oxygen-active dopants (Sc, Y, La) are generally the most sulfur-active, while Ti, Zr, Hf are also quite carbon-active. Low solubility in Ni is another attribute of both effective RE and S segregants, increasing the chemical activity differentials that drive segregation to surfaces. The theoretical and experimental thermodynamics of interface segregation and ‘sulfur-gettering’ have been addressed [65, 66]. While RE-oxides are always more stable than corresponding sulfides, the potential for stable oxy-sulfides also exists and are sometimes observed at nominal sulfur levels or in heavily S, Zr co-doped NiAl, NiCrAl alloys. But under most conditions, the ppm amounts of sulfur available is so small that a widespread distribution of particles is not easily observed.

It was also shown that desulfurization by hydrogen annealing reduced sulfur segregation. Figure 7 shows high temperature angle resolved XPS results for the superalloy PWA 1480 (12 ppma S) producing measurable sulfur surface segregation, but much lower for a hydrogen annealed sample (0.02 ppma S) [67]. (This weak level was associated only with sulfur originally trapped below the native surface oxide, decreasing to zero sulfur at 1100 °C). It is therefore expected that low sulfur

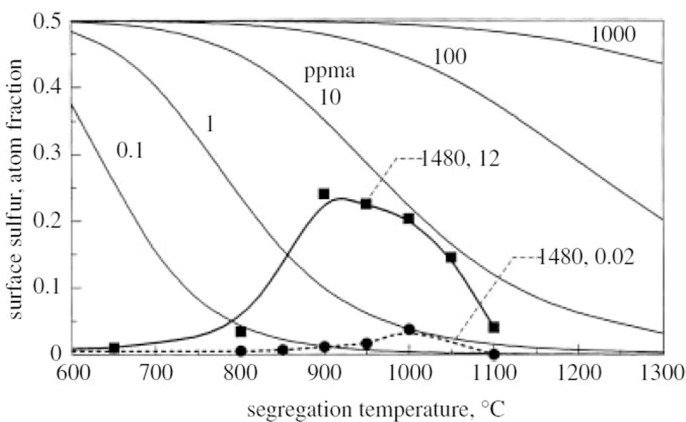


Fig. 7 Temperature dependence of sulfur segregation levels. Symbols for angle-resolved XPS segregation for PWA 1480, as-received (12 ppma) and hydrogen annealed (0.02 ppma), compared to those predicted from Langmuir-McLean isotherm for Ni with 0.1 to 1000 ppma S [67, 92], Miyahara et al., 1985

alloys would not exhibit interfacial segregation, as predicted, and could not then form voids or otherwise weaken the oxide-metal bond. The correlation of greatly improved cyclic oxidation behavior with decreasing sulfur content will be addressed in a subsequent section on single crystal superalloys. Other contaminants such as P and C were also suspected adhesion factors but were never consistently observed at the interface or affected by doping. Hydrogen annealing can remove C, even in the presence of Hf.

While sulfur segregation on a free surface was directly enabled by high temperature Auger and XPS, the anticipated interfacial segregation under actual scales was more problematic, needing refined and pioneering interfacial techniques. Sulfur segregation at thermally grown Cr_2O_3 and Al_2O_3 scale-metal interfaces have initially been documented by difficult cross-sectional STEM [68]^(OM-100), [69], involving a sandwich of oxidation strips held together by epoxy, taking 100 μm slices, dimpling to 20 μm , and masked ion thinning. This process was further complicated by the sublimation of sulfur under the electron beam, making detection difficult or at least fleeting. Scanning Auger microscopy in-situ scale scratching techniques were also applied to this problem by Hou [70]^(OM-100). She produced twenty or so related contributions over the next decade culminating in her scholarly review of the subject [66], concluding:

“S is the only nonmetallic impurity that consistently segregates at the growing $\alpha\text{-Al}_2\text{O}_3$ interface; its presence weakens the interfacial strength. With NiAl, S segregates to the interface only when the alloy is non-stoichiometric. RE’s prevent S interfacial segregation while RE segregation further increases interfacial strength. S and Cr co-segregate and increase interfacial S, while Pt eliminates it (for $\beta\text{-NiAl}$) or reduces it (for γ/γ').”

For example, the relation between Al_2O_3 scale interfacial (tensile pull) strength and sulfur chemistry underlying scales is shown in Fig. 8 for two Ni40Al and Ni50Al ingots oxidized at 1000 °C, each with 2–6 ppm S bulk

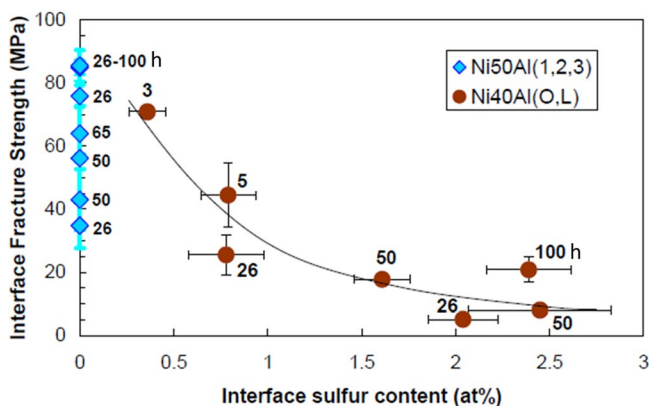


Fig. 8 Decrease in Al_2O_3 scale—NiAl interface strength with interface sulfur content. Oxidation at 1000 °C for times in parentheses; tensile pull test; in-situ Auger chemistry from scratch test [71]^{OM 100}

[71] (OM-100). The stoichiometric NiAl compound revealed no sulfur, regardless of oxidation time. The sub-stoichiometric Ni₄₀Al compound produced a trend of decreasing bond strength over regions exhibiting increased sulfur, generally with oxidation time. Other details abound, but Hou's studies conclusively identified significant segregation from ppm levels of sulfur impurity as the primary source of interfacial weakening, i.e., the root cause of scale spallation in cyclic oxidation of alumina-formers. Her subsequent succinct summation of the state-of-the-art is also noteworthy [72], with most precepts reiterated here.

More recently, nano-SIMS mapping combined with FIB-STEM line scan techniques lend themselves to more widespread documentation of sulfur interfacial segregation, specifically, for a YSZ TBC on a NiPtAl bond coated single crystal CMSX-4 superalloy, after 100 h oxidation at 1150 °C [73]. Sulfur interface segregation, migration through the scale and TBC and segregation on internal Al₂O₃ grit particles in the bond coat were shown. Sulfur was also identified to preferentially segregate on or nucleate interfacial voids, in line with stronger segregation on free surfaces compared to interfaces. The concept derives from lower surface energy sulfur-terminated surfaces compared to clean Ni or Al₂O₃ [74, 75]. Furthermore high-resolution STEM and APT have identified more interfacial sulfur as compared to adherent scales formed from ingots melted in gettered CaO crucibles (superalloy TMS-238 after 1 h oxidation at 1100 °C) [76]. The adherence effect was presumably produced only by sulfur gettering, as no Ca segregation was observed.

Surface energies can be surveyed from a database: (mavrl: crystalium materialsvirtuallab.org) [77] With sulfur surface energies at just 0.01 J/m², the nucleation of free surfaces is favored as compared to clean Ni (2.09–2.40 J/m²) or (0001) Al₂O₃ surfaces (2.13–3.5 J/m²) [78]. By comparison, RE surface energies are intermediate and not especially low, e.g., Y: 1.00; Zr: 1.57; or Hf: 1.72 J/m². (Pt surface energy is 1.60 J/m² and also intermediate between S and Ni or Al₂O₃). Therefore, any surface energy driving force for RE segregation may be secondary to their low solubility (high activity) in Ni. Voids are considered unnecessary for spallation, even though they are, by definition, sufficient. Outward Al flux is generally cited as the root cause for vacancy injection into the interface. Scale wrinkling may exacerbate void formation, and vacancy annihilation at dispersoids may ameliorate the condition. Ultimately, the relative additional RE contributions to adhesion from restricting outward growth or annihilating Al vacancies, compared to concurrent RE interfacial segregation and strengthening, is obscure.

RE doping can therefore produce simultaneous effects of reduced outward (Al) growth, void prevention, RE interfacial strengthening, and sulfur gettering. Separating any primary adhesion factor for doped alloys is problematic. RE ion implantation and incorporation into just the scale may only preferentially affect growth direction and vacancy injection, but concurrent RE interfacial strengthening cannot be discounted. And since most 10¹⁶–10¹⁷ ion/cm² fluences penetrate ~ 10–100 nm, some subsurface substrate interactions with sulfur cannot be ruled out. In any event, the beneficial effects are relatively short lived since the RE supply is limited and diluted by the growing scale [79].

RE-S Counter-Doping and Critical Ratios

The relative amount of bond strengthening, by RE segregation alone, is always obscured by concurrent prevention of sulfur segregation. However, the converse is not true, i.e., bond weakening by sulfur doping is clearly able to overpower RE effects in cyclic oxidation tests. Specifically, Y added as 0.15 wt% Y_2S_3 to **NiCrAl** was ineffective in producing adhesion (based on 1000 h cyclic oxidation at 1050 °C and 300 h at 1180 °C) [28]. Similar ineffective counter-doping results were obtained for **NiCrAl–0.3Y–0.2 S** (wt%) [29] ^(OM-100). As well as S co-doped with Y, Ce, or Hf [80]. Another work demonstrated that Zr needed to be titrated at a higher level to restore adhesion to S-doped alloys, if at all, based on 1100 °C cyclic oxidation of ten Zr/S co-doped **Ni–15Cr–13Al** (wt%) alloys [81]. For alloys doped with 0.1 at.% Zr, producing adherent scales, only 0.01 at.% S was needed to significantly degrade scale adhesion. Alternately, for alloys doped with 0.1 at.% S, 0.3 at.% Zr was insufficient to restore adhesion. An empirical relation, $Zr \geq 600 S^{0.2}$ (atomic) was interpolated to define the onset of adhesion, but only up to 40 h of cyclic oxidation at 1100 °C. This Zr/S relation exceeds that expected for a simple ZrS stoichiometry and implies a much stronger effect of sulfur compared to Zr. On the other hand, at lower sulfur levels ~5 ppmw, **René N5** samples at 10 different Y dopant levels produced essentially the same behavior over 10–100 ppmw Y. Basically a Y/S ratio of just 1:1 atomic was sufficient to provide scale adhesion based on nominal weight changes of only ± 1 mg/cm² after 1000 1-h cycles at 1150°C [82]. While hydrogen annealing could not desulfurize any Y-doped alloy, some improvements in moisture-induced spallation were noted, possibly by simultaneously decarburizing from ~500 ppmw to ~100 ppmw C. Finally, **NiAl** co-doped with 1.0 wt% Dy and 0.002 wt% S maintained a clean oxide-metal interface in an in-situ Auger scratch test after 2 h oxidation at 1200°C [83]. Neither was there any wrinkled scale. The opposite was true for nominal (undoped) and 0.003 wt% sulfur-doped **NiAl**. Thus, the effective Dy/S ratio was again quite high, ~500:1 on an atomic basis. These RE-S counter-doping studies indicate that RE doping is less effective for intentionally S-doped alloys.

One other study questioned the priority of sulfur segregation to adhesion. An undoped **Fe₃Al** alloy (as-received and hydrogen desulfurized) failed to exhibit interfacial sulfur segregation in an Auger in-situ scratch test of a *transition* alumina scale formed at 1000 °C for just 10 min [84] ^(OM-100). However scale spallation was documented for both, even where no segregation was observed, suggesting that the interfacial bond was inherently weak. This was in contrast to an extremely adherent scale formed on **Fe₃Al** doped with 0.1 wt% Zr. It is not clear how these special observations for transition alumina scales on **Fe₃Al** may be generalized to stable α -**Al₂O₃** scales on **FeCrAl**, **NiCrAl**, **NiAl**, or single crystal superalloys. There is a general belief that sulfur does not especially segregate at transition alumina or Ni, Cr, Ta-rich cubic transient scales (often crystallographically coherent with cubic metal) interfaces as compared to (incoherent) interfaces with rhombohedral α -**Al₂O₃**.

Low Sulfur Alloys: From Critical Experiments to Commercial Alloys

While some circumstantial evidence exists for RE bond strengthening, the disentanglement from sulfur gettering effects is problematic. One uncomplicated approach is to examine adhesion for alloys having low sulfur contents and no RE. This has been accomplished with dopant-free alloys by using higher purity reagents for alloy preparation, repeated oxidation/segregation/polishing (purging), hydrogen annealing, and CaO desulfurization in the melt (via Ca-based flux or crucibles). Some examples are mentioned below. The eventual outcome is that commercially available low sulfur engineering alloys (single crystal superalloys) have been produced that demonstrate equivalent cyclic oxidation resistance to Y-doped alloys if the sulfur content is ≤ 0.3 ppmw. Initially these effects were demonstrated over a few cycles to a few hundred cycles of enhanced scale adhesion. It could be argued that the mechanism is operative but perhaps not fully comparable to long term RE-doping effects. But some low sulfur alloys maintain scale adhesion for thousands of hours and enable cyclic oxidation behavior equivalent to RE-doped counterparts.

Initially, there were a handful of oxidation studies that utilized low sulfur alloys. High purity Ni, Cr, Al reagents were used to reduce the as-cast sulfur content from ~ 25 ppmw to $\sim 1\text{--}2$ ppmw [85]. This considerably improved the 1100°C cyclic oxidation resistance. Also, twenty-five oxidation/repolishing purging cycles were used to decrease the sulfur content in NiCrAl from ~ 10 to ~ 3 ppmw. Subsequent 1120°C cyclic oxidation resistance was also clearly improved for 25 1-h cycles [86, 87]. While these studies initially illustrated the point that just reducing sulfur content without RE additions improved scale adhesion, the approaches were somewhat cumbersome and preliminary. Based on the success of Lees et al. using hydrogen annealing to improve Cr_2O_3 scale adhesion on Cr [1], we introduced a similar process for NiCrAl and then for 1st generation single crystal superalloy PWA 1480 alumina-formers, the latter inspired by Smeggil and efforts at UTRC [88–90]. Initially, a certified hydrogen facility was employed using dry 1 atm H_2 and 100 h furnace anneals over $1000^\circ\text{C}\text{--}1300^\circ\text{C}$. Sulfur reduction by hydrogen annealing improved the 1100°C cyclic oxidation behavior: for NiCrAl, the 200 h weight loss was reduced from -23 mg/cm^2 to just -3 mg/cm^2 [43]. For PWA 1480, the sulfur contents of were reduced from 11 ppmw to ≤ 2 ppmw. The corresponding cyclic oxidation resistance behavior was increased accordingly, from -7.8 mg/cm^2 losses after 200 1-h cycles, to a gain of $+0.4\text{ mg/cm}^2$. (Cyclic 1-h polishing/purging was not successful in desulfurization because of a long-term (~ 15 h) transient (Ni, Cr, Ta) oxidation period during which segregation was apparently not prominent. A longer term 24-h polishing cycle was much more effective after the Al_2O_3 -metal incoherent interface had been established) [91].

Eventually, successful desulfurization was demonstrated using a more convenient 5% H_2 -Ar laboratory-scale furnace, allowing for higher throughput and flexibility. One emphatic example is presented in Fig. 9 for 2nd generation single crystal superalloy René N5, with Re and Hf but no Y, hydrogen annealed at 1280°C for 100 h. “The un-annealed” sample (3 ppmw S) lost 23 mg/cm^2 after 500 1-h cycles of oxidation at 1150°C and eventually degraded rapidly via a complex multiphase scale. Hf was clearly ineffective here. In contrast, a sample that was hydrogen annealed

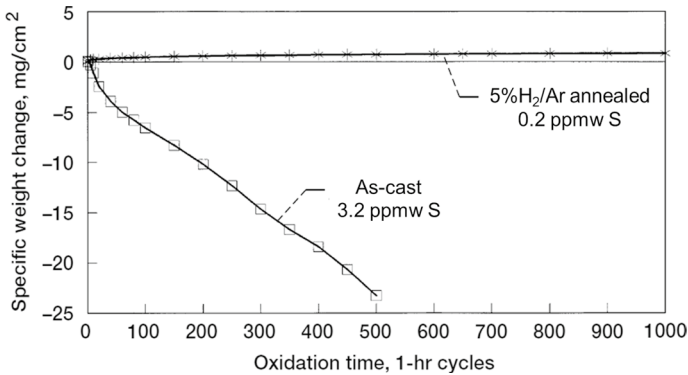


Fig. 9 Extended 1000 h, 1150 °C, cyclic oxidation scale adhesion produced by desulfurizing René N5 (no Y), (from 3.2 to 0.2 ppmw by hydrogen annealing at 1280 °C for 100 h) [92]

(0.2 ppmw S) *gained* only 1 mg/cm² after 1000 h and produced a uniform scale with no spalling to bare metal [92]. Furthermore, the scale thickness can be projected as being only about 5 μm. The remarkable long-term, high-temperature, cyclic performance of this hydrogen annealed superalloy underscored the significance of reducing ppm levels of the sulfur impurity. Another related study attempted to optimize the Y/S ratio in René N5 for 10 levels of Y-doping over 10–100 ppmw [82]. Hydrogen desulfurization of the undoped alloy was more effective than Y-doping and more resistant to moisture-induced spallation (see below). On the other hand, the lowest levels of Y were apparently so effective in reducing the sulfur activity, that these doped alloys could not be desulfurized (~5 ppmw) by hydrogen annealing.

We had also undertaken a parallel extensive study to establish critical sulfur levels needed to achieve scale adhesion for a first generation single crystal superalloy with no Re, Hf, or Y [93]. PWA 1480 samples with 28 levels of sulfur were produced by hydrogen annealing coupons of varying thickness (5), times (4) and temperatures (4). Cyclic oxidation screening was performed at 1100 °C for 500–1000 1-h cycles. Figure 10 shows the time to cross zero weight change, t_0 , as a representative measure of adherent behavior. A 7× step function increase in ‘adhesion life’ occurred as sulfur content was reduced from about 7 ppmw (as-received) to below 0.3 ppmw (hydrogen annealed) [94]. It can be concluded that little further advantage is produced at sulfur levels below about 0.2–0.3 ppmw. For the sample thicknesses employed, this total bulk level is consistent with about 1 S atom per Ni surface atom. It is also consistent with levels of sulfur projected (Langmuir-McLean isotherm) to segregate to the surface at ≤1% of the saturation level (Fig. 7). Both factors are believed to assist in minimizing interface segregation.

More recently long-term durability was demonstrated for another ultra-low sulfur (0.12 ppmw) single crystal superalloy, AM1+0.06% Hf. It gained a maximum of only 0.8 mg/cm² after 3500 1-h cycles at 1100 °C, Fig. 11 [95]. The cyclic weight change behavior was modeled and fitted with a spall fraction (probability, p) of just 0.02% per cycle. The base alloy was Ni–12Al–9Cr–7Co–2Ti–3Ta–2W–1Mo (at.%), with minor dopants and impurities of 570Hf–25Zr–0.12S–23C (ppmw). It also

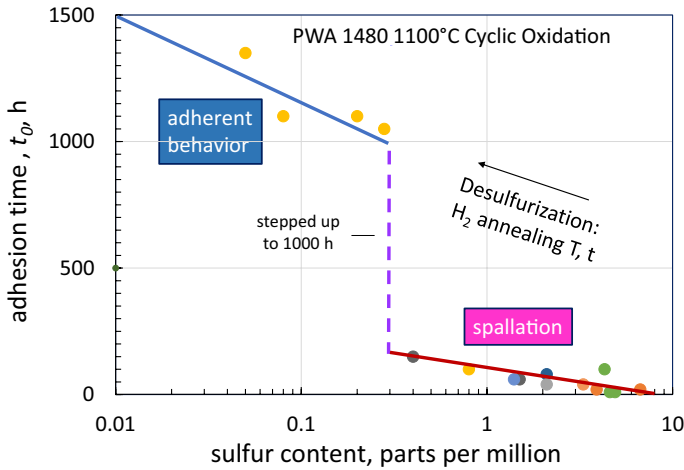
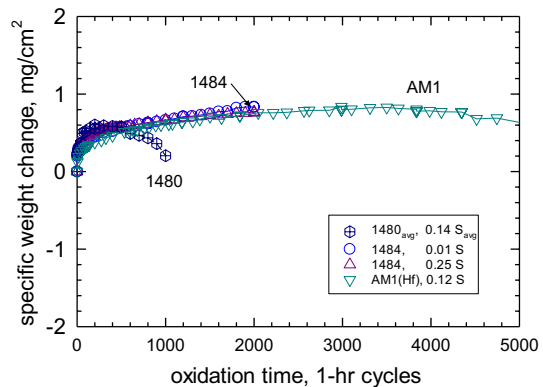


Fig. 10 Sulfur guidelines for Al_2O_3 scale adhesion on PWA 1480 showing abrupt transition at ~ 0.3 ppmw S. Based on 1100°C cyclic tests; desulfurization control by hydrogen annealing. t_0 refers to time to cross zero weight change due to spallation losses [94]

Fig. 11 Low weight gains indicate excellent scale adhesion for ultra-low (< 0.3 ppmw S) sulfur superalloys in 1100°C cyclic oxidation test (PWA 1480, PWA 1484 [93]; AM1 [95])



survived ~ 7000 cycles at 1100°C before exhibiting a weight loss. Further testing to 10,000 cycles produced only a 2.5 mg/cm^2 weight loss. These and other low S (≤ 0.3 ppmw) single crystal data had been summarized [94]. (Note that all the weight changes shown in Fig. 11 are extremely small. PWA 1480 at nominal 7 ppmw sulfur levels loses about $10\text{--}20\text{ mg/cm}^2$ after just 200 h, as compared to a small 0.2 mg/cm^2 gain after 1000 h for low sulfur 1480). In review, it appears that the cyclic oxidation behavior of ultra-low sulfur superalloys is excellent and generally equivalent to that of Y-doped superalloys.

Dramatic improvements in cyclic oxidation resistance have now been demonstrated for most single crystal superalloys by major turbine engine corporations and alloy suppliers world-wide (General Electric, Pratt and Whitney, Rolls Royce, Safran, Siemens, Precision Cast Components, Howmet, Canon-Muskegon,

Mitsubishi MHI, etc.). Desulfurization is typically accomplished for commercial superalloys by melt-desulfurization using CaO sulfur-active fluxing compounds. Ultra-low sulfur levels, similar to those targeted above by laboratory hydrogen annealing (0.1–0.3 ppmw), are now available commercially. Melt desulfurization has been preferred to Y-doping because of Y reactivity with casting crucibles and molds. Problems stemming from RE dopant compositional inhomogeneities or inclusions are also avoided. Interestingly, Hf, Zr, Ti alloying elements, already present in many 1st and 2nd generation single crystals, have not posed these types of problems. It may be due to their higher solubility in Ni alloys compared to Y, for example. Also, while expected to be sulfur-active getters to a high degree, they have not worked nearly as well as Y to improve scale adhesion for single crystal superalloys as compared to the success for Hf, Zr, (and occasionally Ti) doping for NiAl, NiCrAl, CoCrAl, or FeCrAl alloys. There are strong indications that Hf may help prevent carbon effects and improve scale adhesion for 2nd generation single crystal superalloys compared to 1st generation alloys without Hf. Finally, it is also recalled that the critical Zr/S atom ratio to achieve some adhesion in NiCrAl alloys was high at $Zr = 600 S^{0.2}$ [81]. Fitting this to the AM1 superalloy sulfur level of 0.12 ppmw S (0.2 ppma) yields a required dopant (Hf) level of ~430 ppma (~1300 ppmw), on the order of the actual 570 ppmw Hf content. Whether this criterion derived from Zr-doped NiCrAl applies quantitatively to Hf-doped superalloys is speculative. Overall, it appears that considerable adhesion can be achieved for single crystal superalloys at low sulfur levels without Y, Hf, or Zr. Some guidelines for optimum behavior can be inferred from critical RE/S ratios.

Overall, regarding chemical bonding mechanisms, it is therefore concluded that:

Control of sulfur segregation is necessary, while RE-doping is not necessary for considerable adhesion. Further (secondary) strengthening by RE-doping may occur, but is not necessary for adhesion. Sulfur doping RE-doped alloys is sufficient to produce spallation.

Pt Effects

The excellent oxidation resistance of Pt–Al and Ni(Pt)Al alumina-forming alloys is well established. Early works by Felten and Pettit on Pt–Al and Pt–NiCrAl alloys illustrated exclusive alumina scale growth kinetics and excellent adhesion, initially citing pegging as the adhesion mechanism, about a decade before the subsequent discovery of sulfur effects [52, 96]. Similarly, PtAl alloys (exhibiting an interfacial Pt₅Al₃ depletion zone) were studied with Zr dopants [97]. While the undoped Ni(Pt)Al alloy exhibited similar kinetics, but better cyclic oxidation resistance, compared to Pt-free NiAl, both Zr-doped alloys presented lower growth rates and much improved cyclic oxidation resistance compared to undoped alloys. Zr segregation at the interface and at Al₂O₃ grain boundaries was documented in STEM-EDS analyses of the cross-sections.

Pt effects have followed RE effects in terms of focused scholarly studies (~200 references) and intriguing material phenomena. Much of the motivation stems from the commercially important success of widely applied Ni(Pt)Al aluminized

bond coats to protect superalloys. Here 5–10 mg/cm² of electroplated Pt, usually followed by vapor deposition of Al, results in a 25–50 μm Ni(Pt)Al coating with greatly improved environmental protection of superalloy substrates. Pt clearly improved Al₂O₃ scale adhesion and has become the standard of comparison for state-of-the-art turbine airfoil bond coats. Pt counteracts the effects of sulfur impurities introduced from the vapor deposition process, often associated with Al₂O₃-NiAl void formation [98]. Failure mechanisms were also associated with cyclic scale growth/CTE mismatch stresses that drove as-processed alumina coating grain boundary ridges and rumpling of the ductile coating, forcing the overlying scale to crack and detach from these coating apexes. More recent processing advances include Hf and possibly Si doping. In bulk alloys, Hf and Zr are well known to improve scale adhesion and greatly improve high temperature creep. They therefore presumably reduce the ridges/ rumpling/spalling phenomenon, leading to improved TBC top coat life, i.e., more than doubled (> 2000 h) for 1135 °C cyclic furnace tests of MDC150L [99].

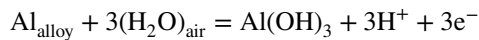
The works of Gleeson et al. [100] have provided a sustained basic scientific thrust in the Ni(Pt)Al area: The beneficial effects of Pt derive from the propensity of Pt to occupy Ni sites on the Ni₃Al lattice and Pt subsurface enrichment that increases the Al activity gradient. This encourages Al diffusion; both favor Al₂O₃ formation in preference to NiO. There is some indication that Pt lessens interfacial void formation which would improve adhesion. Also, Pt affects sulfur segregation as studied by the in-situ Auger scratch test: “Pt eliminates S segregation at alumina/β-NiPtAl interfaces and reduces it when the alloy is the γ/γ’ phase. The effect of Pt can be overwhelmed by the co-segregation of S with Cr [101].” Further demonstration of scratch-induced spallation without massive void formation, but with S segregation, was made for Pt-free NiAl coatings on CMSX-4, but with no S segregation for NiPtAl coatings [101]. The means by which Pt retards or repels sulfur is a point of discussion. While there may be anecdotal belief that sulfur impurities segregate on pure Pt as well as on most metals, specific or direct studies are not widespread [102]. On the other hand, it is reported that S-rich localizations, ~5 μm dia., are observed below the oxide-metal interface for NiPtAl bond coats on superalloys [103]. In that study, imaging SIMS combined with novel back-side thinned sputter profiles have been used to characterize sulfur distributions in an oxidized (coated) superalloy. Oxide-metal S segregation was again observed for NiAl, but not for NiPtAl coatings, nor for low S (0.14 ppmw) uncoated AM1. This confirms the previously cited in-situ scratch test study showing that S segregation, observed for Pt-free NiAl coatings, was prevented for Ni(Pt)Al coatings.

While not arriving at all-encompassing conclusions regarding a first-order (Pt–S) adhesion mechanism, it is important to be aware of these significant Pt effects. To that end, it is of interest to point out the recent development of a Pt-modified single crystal superalloy [104]. In addition to improved mechanical properties, with low Re and no Ru, the alloy boasts oxidation kinetics similar to 2nd generation single crystals. Pt effects will be further addressed in the discussion of ab initio oxide-metal works of adhesion.

2nd Order Moisture Effects

This section introduces other anomalous, perhaps enigmatic, anecdotes related to moisture effects on enhanced interfacial Al_2O_3 scale spallation after cooldown of marginally adherent, stressed scales. It was first observed when undoped NiCrAl was progressively desulfurized by repetitive oxidation/polishing [87]. As the scale became adherent enough to first be retained on cooling, it then ‘unzipped’ when subjected to wet emery paper just before the next polishing treatment. With a few more desulfurization cycles, the scales became resistant to moisture induced spallation. Subsequent studies employed a ‘breath test’, full water immersion, immersion acoustic emission, and high temperature water vapor. A summary of observations and literature review had been provided [105], as described later. Despite the striking manifestations of this decohesion phenomenon, cyclic oxidation in water vapor (and under combustion environments) surprisingly fails to exhibit much of a moisture effect, either on Al_2O_3 growth or spallation for *adherent* scales formed on doped NiAl(Hf) or NiCrAl(Hf,Y) [106]. Furthermore, four low sulfur single crystal superalloys had been shown to be insensitive to moisture with no cracking or spalling of the Al_2O_3 scale. But, if they contained > 1 ppmw sulfur, then the degradation rate was increased by a factor of two in water vapor [91].

An analogy had been drawn between moisture-induced delayed spallation (MIDS) and moisture-induced hydrogen embrittlement (MIHE) of Ni_3Al , Fe_3Al , and FeAl intermetallics [105]. These aluminides were characterized by intergranular segregation of hydrogen extracted from ambient humidity. It was exacerbated by the presence of sulfur and residual tensile stress in the metal, producing delayed (but rapid!) crack growth and failure at room temperature. For example, moisture-induced hydrogen embrittlement was described according to [107, 108]:



Hydrogen embrittlement was therefore proposed as a potential trigger for moisture-induced delayed spallation (MIDS) and desk top spallation (DTS) of TBCs. Water drop/spray experiments were used to record ‘exploding’ TBCs that sustained high TGO strain energy [109]. This failure is believed to be a vestige of the same moisture-induced (H) sensitivity. Indeed, as a demonstration of the hydrogen factor, adherent, mature Y-doped scales on René N5 + Y (1150 °C, 1000 h) were stripped interfacially by cathodic hydrogen charging [105]. While dramatic, this circumstantial result does not directly confirm that hydrogen played a role in MIDS. To further characterize Al_2O_3 -Al-H interactions, S. Hayashi used GDOES sputter profiling to directly identify H at the interface of thin scales formed on René N5 + Y. While some interface H was indeed profiled at the oxide-metal interface, there was no clear difference between moisture-treated and non-treated scales. An updated review of circumstantial evidence above has since been presented, albeit without ‘smoking gun’ proof of moisture-induced hydrogen [108].

One final observation deals with G. Hultquist’s correlation of hydrogen produced from ambient humidity (extracted from elemental metals, equilibrated over 20 years) with the free energy of formation of the metal oxide. H was extracted by meticulous

and calibrated thermal desorption up to 900 °C under high vacuum conditions [110]. The H mass spectroscopy signal was summed and converted into total hydrogen content. It is seen in Fig. 12 that total H release increased with the oxygen reactivity of the metal. The temperature at which the H-peak was released also increased with oxide stability. Thus, hydrogen reactivity (bonding) appears to correlate with oxygen (and thus sulfur) reactivity as well. Whether reactive element H-gettering occurs, similar to reactive element S-gettering, or how it may ameliorate moisture sensitivity for scale adhesion is speculative, but the parallels are intriguing. Hydrogen is known as the ‘stealth embrittler,’ because it is mobile at room temperature, difficult to retain and detect in post-mortems. H-trapping, artificial H⁺ or H₂ injection, and theoretical models offer alternative approaches. Some further discussion of H is included in the next section.

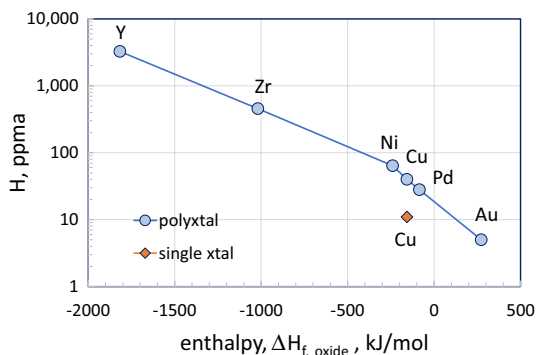
Atomistic Modeling Studies of Oxide-Metal Bonding

Theoretical Results Ideally, theoretical quantum chemistry molecular orbital or density functional theory (DFT) should offer insights regarding oxide-metal bonding. While a few early efforts originated via small cluster techniques, the availability of DFT software has enabled a more widespread effort. Given the elusiveness of direct experimental characterizations of the scale-metal bond strength, corroborations via *ab initio* modeling are appreciated.

Al₂O₃–metal bond energies were addressed by Johnson and Pepper, then Anderson et al. [111, 112]. In general, the Al₂O₃–metal bond was found to increase according to the free energy of formation of the metal-oxide due to hybrid electron orbitals allowed by unfilled metal d-shells. In cluster models, it was found that a Y-dopant formed a strong bond to both Ni metal clusters and AlO₆ oxide clusters, about twice that of corresponding Al–Ni bonds or AlO₆–Ni, or –Al bonds. Furthermore, S-contaminated interfaces were predicted to decrease bond strength [113]. The binding of Al₂O₃ to clean Ni(111) was projected to be markedly stronger than a p(2×2)S covered Ni(111).

Another decade of experimental alloy sulfur variation and surface analytical verifications provided the backdrop for high-performance computing approaches to scale-metal adhesion by Carter, Smith, Chen, Zhang, and Sloof et al., as considered

Fig. 12 Hydrogen trapping correlation with metal-oxide stability: Thermal Desorption Spectroscopy (TDS) of pure metals aged for 20 y at ambient; (cumulative TDS over 12 h, from 25° to 900 °C in 50 °C steps) [110]



below. “The local bonding at the interface led us to investigate (reactive) elements with open *d*-shells that could be added to the bond coat alloy to promote stronger interactions at the interface. We perform spin-polarized DFT calculations using the Vienna Ab Initio Simulation Package (VASP). ... in both the *local density approximation* and the *generalized gradient approximation* to DFT for certain test cases. ... [114]” They reported clean interface strengths (0.62 J/m^2) increased ($> 5x$) for dopants at the Ni(111)/Al₂O₃ (0001) interface: to 3.35 for Sc, 3.24 for Y, 3.68 for Ti, and 3.21 for Zr (in J/m^2), summarized in Table 2 and compared graphically in Fig. 13. According to this series, transition metal dopants with unfilled d-shells are again expected to improve the Ni/Al₂O₃ bond, i.e., scale adhesion, as presaged by Johnson, Anderson et al. [111, 112]. Based on interface strengths here, Ti showed the greatest increase, but is generally not effective experimentally, except in FeCrAl. 1–2% Ti is not effective in practice and may be considered detrimental to overall oxidation resistance of many alloys. Next, Sc, not often studied, had been effective in FeCrAl [14]. Third, Yttrium is generally the most powerful dopant (likely equivalent to La and Ac group elements), but not predicted as such here. Finally, Zr and Hf are often effective experimentally in most NiAl, NiCrAl, and FeCrAl substrates and Zr is so indicated here. For single crystal superalloys, ~10–100 ppmw Y appears to be necessary for optimum Al₂O₃ scale adhesion at nominal (5 ppmw) sulfur levels. Some experimental benefit, less than that of Y, may be provided by ~0.1 wt% Hf dopants. Thus many disconnects between theoretical bond strengths and cyclic oxidation results are immediately evident. A subsequent DFT investigation also considered effects of impurities and dopants on adhesive strength of the Al₂O₃(0001)/NiAl(110) interface, including S, Pt, Hf, Table 2 [115]. It was seen that the clean bond strength (0.66 J/m^2) was greatly increased (3x) by 1 ML Hf (2.06), greatly decreased (3x) by S (0.18), and relatively unchanged by Pt (0.53), in J/m^2 .

Table 2 Compilation of theoretical NiAl–Al₂O₃ bond strengths for various RE, Pt, and impurity interfacial dopants

Alloy	Clean	Hf	Zr	Y	Hf+Y	Pt	S	C	Y,Hf+S	Study
Ni	0.62		3.21	3.24						Carter 2002
NiAl	0.66	2.06				0.53	0.18			Carter 2007
Ni	3.20						0.62			Smith 2003
NiAl	1.06	3.21					0.36		1.35	Smith 2008a
NiAl+	3.13	3.21					1.86		1.89	Smith 2008b
NiAl	0.83	1.76		1.05	3.16	0.85	0.27		0.75	Chen 2011
NiAl	0.78	1.34	1.32	1.28						Zhang 2016
(NiAl) ^a	4.84	4.88	4.73	3.56			3.07	3.30	4.08	Sloof 2005
(Al ₂ O ₃) ^a	4.84	6.02	5.86	4.75			2.50	2.21	3.72	Sloof 2006
+Al rich										

Data from DFT studies by Carter 2002, 2007, Smith 2008 (a,b), Chen 2011, and Zhang 2016 et al.; thermodynamic models for undoped and half-couples from Bennett/Sloof 2005, 2006. (111, 110) NiAl and (0001) Al₂O₃ interface planes

^aHalf interface

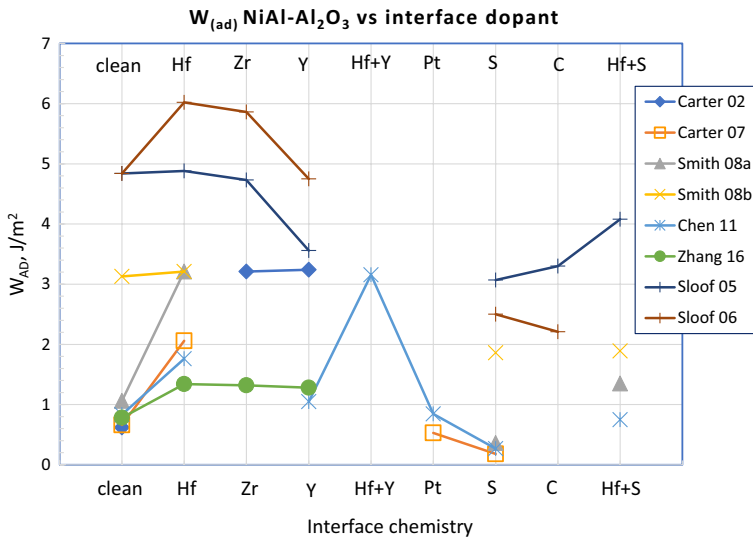
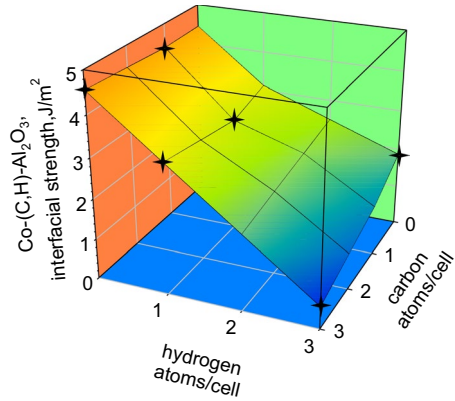


Fig. 13 Overview of DFT calculations of NiAl-Al₂O₃ bond strength as a function of interfacial RE, Pt, and impurity dopants: showing increases, no effect, and decreases, respectively (extracted from multiple sources as shown in Table 2, 2002–2016). (note: trends are more valid within a single study, shown by connecting lines to guide the eye)

The primary question of S segregation and Ni(111)/Al₂O₃ (0001) bond weakening was also addressed by Smith et al. [116]. First-principles computations were also performed via VASP. Multiple Al₂O₃ surface terminations and S positions were considered. They found “...that S substitution for Ni at the interface replaces a strong O-Ni bond by a weak S-O bond... (and) weakening of the intrinsic bonds by the strain needed to accommodate the impurity, manifested as a larger interfacial separation.... The segregation of 1/3 ML S to oxygen-rich interfaces lowers the work of separation from over 3.2 J/m² to under 2.1 J/m², (and to as low as 0.62 J/m² for 1 ML S segregation), consistent with experimental observations of interfacial embrittlement and spalling upon segregation.” Similarly, the same group modelled (110) NiAl/(0001) Al₂O₃ and Hf and/or S segregants. A number of configurations and ML coverages were examined [117]. It was found that the work of separation for the clean stoichiometric interface was 1.06 J/m², decreased to 0.36 J/m² for 2/3 ML of sulfur segregant, increased to 3.21 J/m² for Hf_{Ni}, and moderated to 1.35 J/m² for Hf_{Ni} + S_{Ni} co-segregation. For an Al-rich interface the values were 3.13 J/m² (clean), reduced to 1.86 J/m² for S_{Ni}, increased to 3.21 for Hf_{Al}, and moderated to 1.89 J/m² for Hf_{Al} + S_{Ni} co-segregation. Hf segregation is projected to substantially increase W_{sep} or prevent more serious W_{sep} reductions by co-segregation with sulfur.

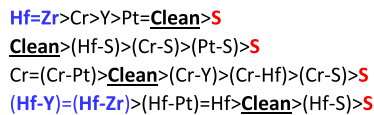
Smith et al. constructed Co-Al₂O₃ interfacial models addressing bond strength as affected by H and C content atop a 2-oxygen atom rhombohedral surface cell [118]. The calculated data, possibly relevant to moisture-induced hydrogen delamination, has been reconstructed and shown as Fig. 14 [108]. Here it can be seen that a significant decrease in bond energy is predicted for an H-segregated interface, with weaker interactions from carbon. Specifically, the work of

Fig. 14 H, C effects on Co–Al₂O₃ interface strength; ab initio calculations for a 2-oxygen atom surface cell; star-points data [Smith 2004] and interpolated 3-D diagram [108]



separation decreases from 4.56 for 3C-0H coverage to 0.56 J/m² as H is increased to 3C-3H coverage. This bond energy decrease is comparable to the 1 ML sulfur detriment.

Another extensive DFT study of 16 dopant configurations of NiAl(110)/ α -Al₂O₃ (0001) bonding was also provided by Chen et al [119]. The work of separation, W_{sep} , was found to increase substantially with Hf, Zr, Y, and Cr dopants and decrease substantially with an S impurity segregant, Table 2 and Fig. 13. Pt substitution for Ni did not affect the clean interface bond strength or remove the detrimental effect of S. Hf-Y and Hf-Zr co-doping produced a notable synergistic improvement, while Hf additions could only partially mitigate the detrimental effect of S. Other Pt, Cr, and S co-doping combinations showed fairly complex, non-linear W_{sep} (J/m²) trends:



Generally, RE co-doping produced the strongest bond, followed by a single RE, then single Cr and Pt. S doping was always the single weakest configuration, and S-RE co-doping was weaker than the clean, undoped interface bond strength.

It is well recognized that Pt foil – Al₂O₃ hybrids form practical configurations as vacuum-tight metal-ceramic seals. Pt does not fit the high negative free energy of oxide formation characteristic of other M-Al₂O₃ bond strengthening RE segregants. Nevertheless, early molecular orbital models revealed higher interfacial strength driven by strong Pt–Al bonds [120], as might be expected from the high congruent melting point of Pt–Al. Given that Pt replaces Ni in Pt-modified NiAl, it is reasonable to expect that a Pt-rich surface might improve the oxide-metal bond. However, this early result was not reproduced by subsequent ab initio calculations, where Pt enriched interfaces produced little change in W_{ad} compared to the clean NiAl–Al₂O₃ interface, Table 2 [115]. It was recognized that a primary role of Pt may be to prevent indigenous sulfur segregation, but that exact mechanism remains unclear. There

is also some indication that Pt may slow sulfur diffusion in NiAl + Pt [121, 122], but not whether this effect is sufficient to curtail sulfur segregation.

Another DFT study by Zhang et al. has been used to model effects of multiple RE segregants on the adhesion energy of the α -Al₂O₃/ β -NiAl interface (Table 2 and Fig. 13) [123]. Hf doping of the interface yielded the greatest theoretical increase in W_{ad} over the clean interface (1.34 vs 0.78 J/m²), with decreasing effects ordered as Hf > Zr > Dy > Y > La. Increased doping levels and RE co-doping were found to increase adhesion values all around. But generally, Y is not observed to be less effective in practice than Hf or Zr for adhesion as predicted here. Significantly, 1200 °C cyclic oxidation experiments of 0.05% RE-co-doped NiAl were also provided in correlation to the theoretical projections. All experimental combinations greatly improved adhesion over undoped NiAl, equivalently, with Y + La co-doping being the least effective. No attention was given to experimental sulfur contents, excessive NiAl grain boundary oxidation, probably associated with RE-Ni precipitates.

Lastly, a “macroscopic atom model” was employed as an alternative to DFT mega-computing approaches. It was used to estimate the work of adhesion between α -Al₂O₃ and β -NiAl and the bonding of these endpoints to Y, Zr, and Hf reactive elements and S, C impurities [124, 125]. The work of adhesion was calculated to be 4.8 J/m² for the undoped NiAl-Al₂O₃ interface, Table 2, Fig. 13. As such, it is not exactly the same as other studies addressing segregants sandwiched between the scale-metal interface. Nevertheless, notable similar trends are illustrated. The Al₂O₃-X interface strength was somewhat increased for Hf (6.0) and Zr (5.9), unchanged for Y (4.8), and reduced for S (2.5) and C (2.2), all in J/m². Similarly, the NiAl-X work of adhesion was roughly unchanged for Hf (4.9) and Zr (4.7), lower for Y (3.6), S (3.1) and C (3.3) J/m². Thus, the primary role of the RE was concluded to be the prevention of bond weakening by scavenging of S impurities (with Y > Zr > Hf effectiveness) or C impurities (with Hf > Zr > Y effectiveness). Some supporting evidence was provided by oxidation tests and X-ray Photoelectron Spectroscopy (XPS) of doped NiAl. The use of a RE-Al₂O₃ half-system rather than the usual NiAl-RE/S-Al₂O₃ segregated interface poses some questions when comparing to other modeling studies, but it can be surmised that the lowest adhesion energy can be taken as the weakest link of the Metal-X-Oxide system, yielding the conclusion that Zr, Hf, and Y have equivalent effects on predicted bond strengthening. Compared to elemental S or C, little difference was observed when using sulfides or carbides as the segregated species, or when using RE oxides as the segregated species, as compared to RE elements. It was recognized that the high solubility of Hf and Zr in NiAl (1 at.%) vs Y (12 ppm) deserves attention in describing experimental evidence and agreement with the model.

Recapping, the theoretical model bond strengths from DFT calculations summarized in Table 2 indicate that the ‘clean’ interface strength varied from 0.62 to 0.83 J/m² for the stoichiometric NiAl interface. Much higher values were obtained for Al-rich NiAl (3.13), for elemental Ni (3.2), and for the macroscopic model (4.8), all in J/m². This suggests that various approaches will produce various results beyond the scope of this work to assess. Variances may arise from using Al or O terminated (0001) α -Al₂O₃ or different epitaxy with (111) Ni or (110) β -NiAl. Effects of Ni or Al interlayers, NiAl stoichiometry, or foreign atom positions may also affect

the results. Nevertheless, in general, RE-segregated interfaces were 2–4× as strong as clean interfaces, whereas S (and C) contaminated interfaces were 2–5× weaker than the clean interface, when compared within individual studies using the same interface definition and model protocols. Positive Cr effects are surprising, but difficult to reconcile with experimental behavior since Cr is largely present in many MCrAl alloys, with no adhesion improvement, but rather shows Cr+S co-segregation. The absence of Pt W_{ad} strengthening effects in two studies has been used, by default, to support Pt–S interactions and diffusion reduction within the bondcoat. However, widespread use of Pt–Al₂O₃ vacuum tight seals suggests bonding may actually be good experimentally, along with high melting point compounds as evidence of strong Pt–Al interactions as well as the early molecular orbital study [120]. The W_{ad} values in the data sets are thus system specific and sometimes difficult to cross compare between studies as invariant properties. This also suggests that comparisons to experimental results, having undefined non-ideal interfacial geometries and chemistries, may be best viewed in relative terms.

Overall, modeling confirmed the experimentally observed beneficial effect of RE dopants and the detrimental effect of sulfur impurities as segregated elements, but not in a strictly linear fashion according to various rankings of W_{ad} . Discrepancies with empirical results may arise for sulfur reactivity differences, solubility differences, and segregation potential, not necessarily addressed by these studies. The double role of RE dopants as bond-enhancers vs sulfur-getters thus continues to be a long-standing question. Overall, these studies suggest roughly equivalent powers of RE strengthening or S weakening, when taken separately. When RE-S co-segregants were addressed, the results were not dominated by either, but moderated by each. Pt is not always indicated to strengthen the interfacial bond, but may curtail sulfur segregation due to undefined Pt–S interactions within the bond coat.

Comparison to Experimental Trends for Doped/Co-Doped Alloys It is now useful to relate the theoretical dopant studies back to wide-ranging experimental dopant results for self-consistent, long-term life tests of 70+ commercial and experimental NiAl, FeAl, NiCrAl, and FeCrAl alloys by Pint [13, 126]. Typical dopants examined were Ti, Zr, Hf, and Y, and some with Pt alloying. An overview of the primary trends is shown in Table 3, summarized in the performance chart of Fig. 15. The legend shows a color-coded matrix with over 12,000 h life at 1200 °C for Hf/Y co-doped FeCrAl as a top performer compared to 300 h life for undoped FeCrAl at the other extreme. Tests generally used 1-h cycles. Life was assessed by (1) time to total mass change breakaway, indicating chemical breakdown due to severe Al depletion, or (2) time, t_0 , for net sample weight to cross zero weight change, indicating accrued spallation. Time-to-breakaway was normalized to sample thickness. It should be noted that time-to-breakaway reflects total inability to reform an Al₂O₃ scale and depends, firstly, on excellent adhesion and, secondly, on total Al reservoir. Interfacial spallation is one degradation factor, but scale and alloy deformation (mechanical and thermal expansion properties) also factor into this extreme durability test. The chart in Fig. 15 suggests best behaviors for FeCrAlY and NiAl-Hf. Y was beneficial to all substrates. Hf and Zr were most beneficial to NiAl and PtAl alloys, whereas Ti was *only* beneficial to FeCrAl. Pt was helpful for NiAl, but not to the high level achieved by reactive ele-

Table 3 Condensed compilation of cyclic oxidation lifetimes for various high performing doped Fe(Cr)Al and Ni(Cr)Al alloys/compounds

T (°C)	Base alloy	Dopants	Life (h)	Criterion	Fig. #; S (ppmw)
1250	Fe-17Al	Ti/Y	> 16,000	BRKWY	42
1200	FeCrAl	Hf/Y	12,500	BRKWY	31
1200	APMT	Hf/Zr/Y	5300	BRKWY	31
1200	APM	Zr	5100	BRKWY	31
1200	PM2000	Y ₂ O ₃	3500	BRKWY	31
1200	MA956	Y ₂ O ₃	3000	BRKWY	31
1200	214	Zr/Y	800	BRKWY	41
1150	NiAl	Hf	12,000	t ₀	35
1150	Ni(Pt)Al	Hf	12,000	t ₀	35
1150	PWA 1484	Hf	> 1000	t ₀	0.10 S
1150	René N5	Hf	> 1000	t ₀	0.01 S
1100	AM1	Hf	7000	t ₀	0.12 S
1100	PWA 1484	Hf	> 2000	t ₀	0.01 S
1100	René N5	Hf	> 1000	t ₀	low S
1100	PWA 1480	none	> 1000	t ₀	0.1 S

From long-term testing compiled by Pint et al. [Shreir's Corrosion, 2010] and SXSA data from data highlighted in this paper. Life based on time-to-breakaway (normalized to 1.5 mm thickness) or time to cross zero weight change

ments. Pint had shown some loose correlation of improved cycle life with the size of the RE ion. Good rule-of-thumb dopant/impurity guidelines were demonstrated for $Y/S > 1$ and $Hf/C > 1$ critical ratios, at least at lower levels. FeCrAl breakaway life was generally much greater than that for NiCrAl alloys because FeCrAl ductility generally accommodates stress relief more so than stronger NiCrAl alloys. It was also significant that higher levels of Hf can be retained in solid solution compared to Y without precipitating phases leading to oxidative excess. Finally, the overarching conclusion was that *any improvement from reduced scale growth rate was less important than improved scale adhesion* in optimizing cyclic oxidation lifetime.

Another group examined RE co-doping effects on the cyclic oxidation of NiAl [127]. Levels of 0.05 at.% were used for single and co-doped Dy/Hf, Hf/Zr, Y/La, and Hf/La, all having 0.1 at.% total RE dopant. Reductions in effective k_p over singly doped alloys were sometimes found for co-doped systems in 100 h, 1200 °C cyclic oxidation. The lowest rate was found for Hf/Zr co-doping (7.4×10^{-7} mg²/cm⁴/s), closely followed by Hf and Zr single dopants. The highest rates were found for Dy, Y, undoped, and La alloys, in that order. An effective ion cluster radius was offered in a diffusion blocking model. However, since growth and spallation amounts were combined to extract an effective “parabolic rate” under cyclic conditions, it was difficult to separate adhesion effects from kinetic effects. Grain boundary precipitation in the alloy, and apparent grain boundary oxidation, was another complication.

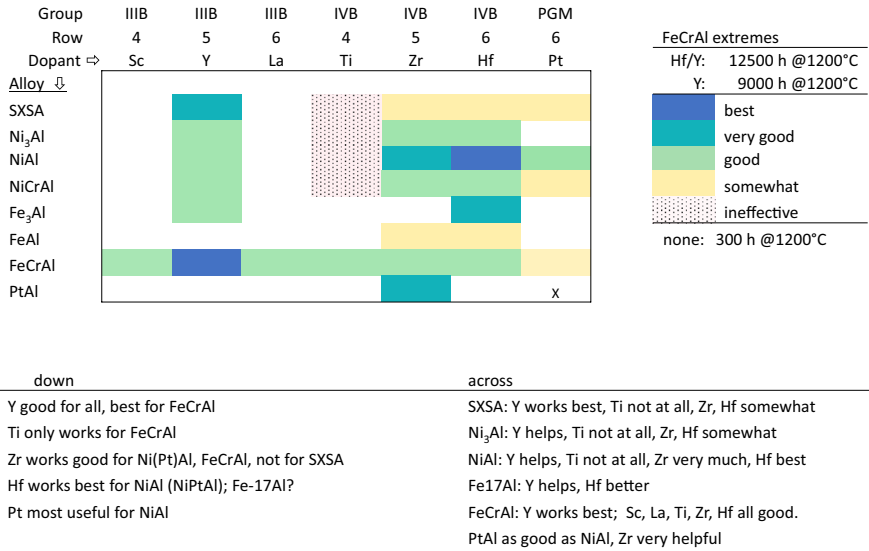


Fig. 15 Performance chart of cyclic oxidation lifetime of various alloys/compounds as a function of RE dopant, largely based on the long-term testing performed by Pint et al. [Shreir's Corrosion, 2010] and from SXSA data presented in this paper. Life based on time-to-breakaway (normalized to 1.5 mm thickness) or time to cross zero weight change. Color coded (pink), from a minimum life of 300 h at 1200 °C for undoped FeCrAl, up to blue for 12,500 h maximum life for Hf/Y-doped FeCrAl (Color figure online)

The theoretical models, at least for NiAl, seem to indicate greatest increase in aluminum oxide-metal bond strength with Hf/Y co-dopants, with Hf as the best single dopant, and Y less effective. One study resulted in the order of Hf > Zr > Dy > Y > La while another reported Ti > Sc > Y = Zr. Pt produced no change. This is mostly consistent with the experimental results showing high life values for Hf-doped NiAl. Less effectiveness for Y is puzzling, but experimental NiAl + Y literature is sparse, except for ion implantation and short exposures. Co-doping was indeed shown to be effective experimentally, but only for other alloys. In contrast, Ti is known to be ineffective for NiAl, while Pt is helpful, especially in commercial aluminide coatings. Thus, predictions from theoretical models are not in total agreement with experimental results. RE effects on sulfur segregation, produced in the alloy, are just as important or more so in practice as is the RE bond strengthening effect predicted for the interface. Modeling sulfur activity in the alloy (segregation potential) as a function of RE additions may therefore be a fruitful avenue to pursue. Alternatively, thermodynamic modeling of RE behavior in the alloy also provides guidance. Gheno et al. have used CalPhaD and Thermo-Calc to describe Hf-doped NiCrAl in order to predict internal HfO₂ formation [128]. Basic trends were identified as a function of Cr, Al, and Hf content as well as O, S, and C levels. Their strategy provides a template to study different alloys and dopants.

Pint also points out the importance of alloy mechanical properties [98]: "...both very strong and very weak substrates are less resistant to spallation. Strong substrates do not dissipate strain energy by creep and thus allow strain energy to build to failure, whereas

weak substrates may be deformed isothermally by scale growth stresses, resulting in convoluted scales which spall on cooling...” Also, with regard to mechanical behavior and modeling of Al_2O_3 , it is recalled that bulk Al_2O_3 creep rates follow the oxygen ion charge [47] (from -1.2 to -1.5), first increasing with Mg and Ti, then decreasing over 3 orders of magnitude according to Sr, Zr, Y, and Y/Zr co-doped Al_2O_3 (“**Growth Stress**” section). These creep trends reflect grain boundary segregation effects on stress-induced grain boundary transport and may have a correlation with diffusivity and corresponding doped scale growth kinetics. Reduced kinetics are helpful from the standpoint of lower strain energy accumulated for extensive (growth) exposures. Outward Al growth with associated vacancy injection may also be reduced. Any direct connection with adhesion is not clear, but it is interesting to point out that Ti (increased Al_2O_3 creep rate) is usually ineffective as an adhesion dopant, while Y and Y/Zr co-doping (decreased Al_2O_3 creep rates) are most effective, in that order. The implication is that doped Al_2O_3 grain boundary structures, electronic transitions, and dopant interactions affecting creep may also be related to those affecting oxide-metal bonding.

Al_2O_3 Scales on MAX Phases—A Curious Footnote

Alumina-forming M-A-X phases present another intriguing, perhaps off-beat, but related topic. Briefly, Ti_3AlC_2 , Ti_2AlC , and Cr_2AlC ceramic compounds are well known to form protective Al_2O_3 scales with kinetics comparable with those formed on metal alloys [129, 130]. Fine grain scales again control the rates by grain boundary diffusion. Protective behavior was observed up to 1400°C . Planar interfaces are more prevalent on the ceramic MAX phases than on more ductile metals, although MAX phase creep strength at very high temperatures is not especially good.

While initial transient oxidation is dominated by TiO_2 formation on the Ti compounds, long term scale growth is dominated by a healing sub-layer of Al_2O_3 . It is unclear how the presence of ample Ti dopant in the scale does not seem to adversely affect subsequent kinetics as would be expected in Ti-containing superalloys or TiAl intermetallics. 1200°C oxidation of Ti_2AlC , without RE dopants, *never* produced spallation for up to 2800 h of interrupted oxidation or during 1000 1-h cycling because of excellent CTE matching with $\alpha\text{-Al}_2\text{O}_3$, ($9.62 \times 10^{-6}/\text{K}$ vs $7.2\text{--}8.6 \times 10^{-6}/\text{K}$) and residual compressive stress under 0.65 GPa [131]. This matching has enabled extensive scale thickness (35 μm) and TBC top coat compatibility on Ti_2AlC with no interfacial failure after 500 h at 1300°C [132]. However, scale or substrate damage makes the compound easily susceptible to runaway oxidation via non-protective mixed $\text{TiO}_2\text{-Al}_2\text{O}_3$ scales [133–135].

The CTE differential is larger for Cr_2AlC ($13.3 \times 10^{-6}/\text{K}$) than for the Ti-based MAX phases. Interfacial spallation is often observed after oxidation at 1200°C , revealing tell-tale interfacial imprints of the Al_2O_3 grains in the substrate [136]. Unlike the Ti MAX phases (which show no depletion zones), the Cr_2AlC substrate forms a deleterious Cr_7C_3 depletion zone, often with entrapped porosity and no Al_2O_3 reformation ability. It is logical that better CTE matching of MAX phases with $\alpha\text{-Al}_2\text{O}_3$ reduce cooling stresses and enable better cyclic scale retention. It also appears that the Ti MAX phases possess high Al diffusivities and stoichiometry adjustments with basal plane faulting compliances that help avoid distinct depletion zones.

A question arises as to whether carbon or sulfur affects scale adhesion for any MAX phases. Prevalent C (25 at.%) does not seem to affect interfacial adhesion. But CO_2 formation may promote void formation in the depletion zone. Also, Cr_2AlC was hydrogen annealed in an attempt to improve adhesion, but sulfur was only reduced to 7.4 ppmw from 9.4 ppmw [134]. Only a slight, short term improvement in scale adhesion occurred, and both conditions were prone to delayed, moisture-induced spallation. Overall, it is clear that CTE matching (Ti_2AlC) has allowed perhaps the longest cyclic Al_2O_3 scale durability on any substrate at the highest temperature (1300 °C), without the use of RE dopants. Other than initial TiO_2 transient oxidation, the exact role of Ti in Al_2O_3 growth and spallation is unclear. This bears some relation to broader scale adhesion issues, but MAX phase behaviors do not necessarily resolve any of the current questions regarding Al_2O_3 -metal adhesion. They are mainly consistent with expectations for a reduced driving force for scale spallation due to lower CTE mismatch stresses.

Final reflections

A point-by-point logic test is provided in the “[Appendix](#)” offering rebuttals or confirmations of various adhesion premises. Based on this assessment, a hierarchy of effects is presented in Fig. 16. First, control (elimination) of sulfur segregation is the only factor found to be both *necessary* and *sufficient* to impart significant alumina

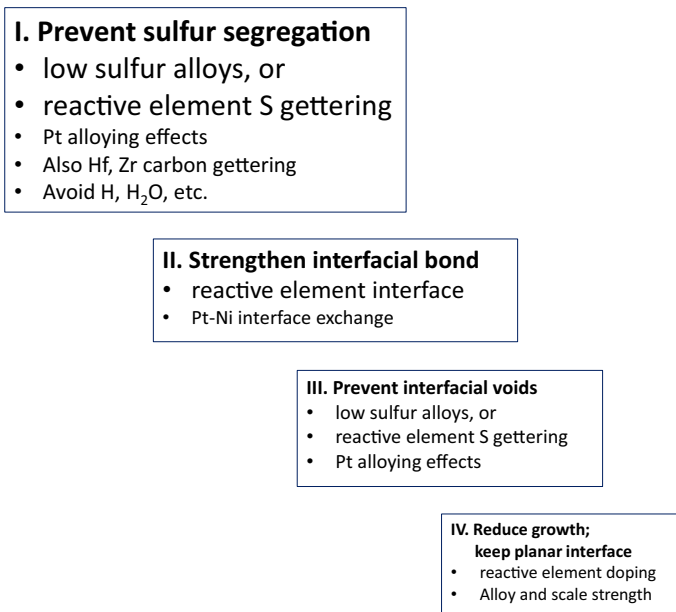


Fig. 16 Hierarchy of scale adhesion factors, ranked by criticality (necessary and sufficient). Sulfur segregation must first be limited by ultra-low sulfur alloys, RE gettering, Pt additions or some combination. RE segregation likely improves the interfacial bond, whereas H, C, (H_2O) may also weaken it. Void prevention is secondarily useful. However, growth rates do not affect interfacial adhesion markedly

scale adhesion. It thus assumes the highest level in the diagram. Second, additional bond enhancement is conferred by RE interfacial doping, but is not required for 1st order effects on adhesion. Third, void control is helpful, but recognized as a result of curtailing sulfur segregation and nucleation promoted by low surface energy. This is more essential than by providing vacancy sinks or reducing Al transport and outward scale growth. Finally, reduced growth rates help to minimize the strain energy in the scale due to CTE mismatch stresses, but cannot itself compensate for an already weak interface. RE dopants may additionally produce strengthening effects in the bulk scale and alloy and thus reduce creep, ratcheting, and buckling, thus helping to maintain a flat interface.

According to such an outline, a recipe for addressing optimal performance based on increased adhesion and long-term cyclic oxidation resistance is offered and presented graphically, Fig. 17. Ideally, a base alloy of very low sulfur is preferred, on the order of 0.1 ppmw (~ 0.15 ppma) or less. Otherwise, reactive element additions should be high enough to decrease sulfur (and carbon) activities, and thus segregation, but not large enough to produce excess oxide intrusions (i.e., overdoping). RE_{III}/S and RE_{IV}/C ratios ≥ 1 , at a minimum, can serve as a guide. It is also useful to consider strategies to maintain a flat interface without undulations and stress

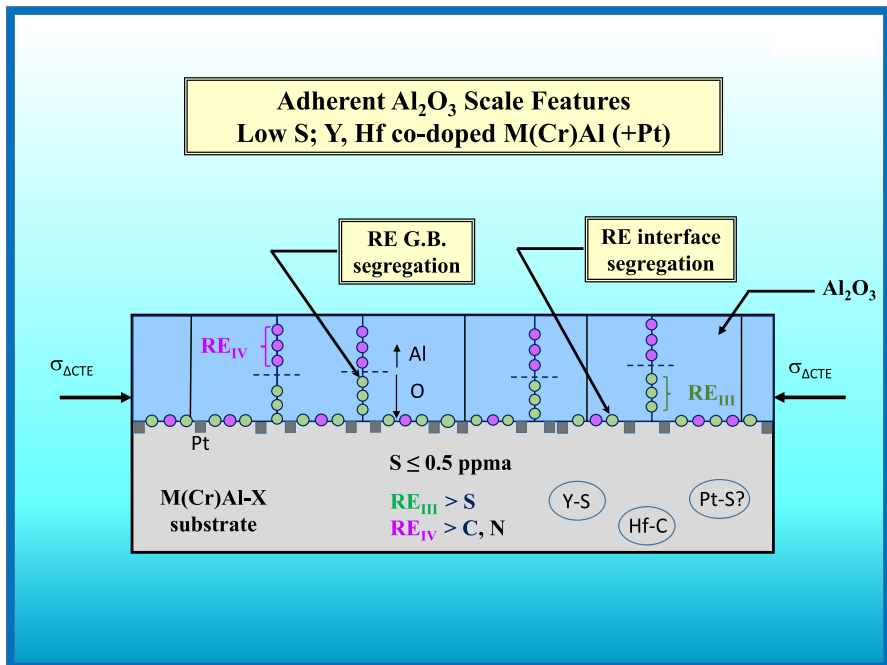


Fig. 17 Schematic of adherent alumina scale features. Low sulfur and RE, Pt-doped substrate to reduce S, C activity and segregation. No sulfur interfacial segregation or voids. RE interface segregation for improved strength; Pt preference to Ni interface for selective Al₂O₃ formation (bonding?). Columnar, inward growing grains with RE segregation to reduce aluminum-outward, oxygen-inward kinetics and increase creep strength

concentrations. Base alloys are strengthened, such as Zr, Hf-doped NiAl, or solid solution strengthened and precipitate hardened superalloys. Here high RE_{IV} solubilities (compared to Y for example) allow for a greater strengthening effect. Similarly, Y, Zr/Y, or Nd/Zr co-doping produce very creep resistant bulk Al₂O₃ (“Scale Plasticity” and “Growth Stress” sections). This could reduce scale ratcheting effects during cyclic exposures. In the other direction, moderately soft alloys could deform at temperature, on cooling, and relax interfacial CTE stresses during more demanding breakaway, long-term oxidation life testing. Here, weaker FeCrAlY may be an asset, in contrast to stronger NiAl-Hf. Co-doping may reduce scale growth via outward Al (RE_{IV} doped) or inward O (RE_{III} doped) grain boundary diffusivity. Reduced scale thickness produces a corresponding reduction in stored elastic strain energy, the driving force for spallation on cooling. Based on limited DFT information, RE_{III}/RE_{IV} co-doping may increase interface strength as well. Some guidelines regarding atomic size or oxygen ‘ionicity’ have been proposed.

An abbreviated overview of the many factors discussed here is presented in Table 4 to broadly scope the ~50 years. history of developments along with any key technology that enabled the observation. Scale morphology, ¹⁸O tracer studies, scanning and hot stage Auger, SIMS, FIB-STEM, sulfur and RE segregation, desulfurization, and DFT all played a role. The broader mosaic of fine features amassed over countless related studies (~1000 from search results) have provided a rich tapestry of adhesion phenomenology and empiricism. All of these characterizations assume various positions of increased characterizations, understanding and benefits.

Table 4 50 year timeline of selected advances to understanding alumina scale adhesion

Technique	Base material	Observation	Era
SEM	FeCrAl	Scale rumpling, voids	1972
SEM	PtAl	Adhesion w/o RE	1976
SEM	CoCrAl	Pegging	1977
SEM	FeCrAl	Equiaxed, columnar grains	1979
Hot stage Auger	NiCrAl	S surface segregation	1985
Sulfur reductions	NiCrAl	Adherence, undoped	1986
X-STEM	FeCrAl	Y interface, g.b. segregation	1987
Hydrogen annealing	PWA 1480	<0.1 ppm S, adhesion	1989
Auger, scratch	NiAl	S interface segregation	1991
¹⁸ O imaging SIMS	Fe–Al, Ni–Al	Inward + outward growth	1992
In-situ Auger scratch	FeCrAl	S interface segregation	1992
X-STEM	NiAl	S interface segregation	1996
PLS	FeCrAl	Direct stress measurement	1996
Re-oxidized wedge	FeCrAl	Inward + outward growth	2005
Imaging SIMS, sputter profile	AM1, Ni(Pt)Al	Sulfur distributions	2009
FIB-STEM	Fe(Ni)CrAl	Y, Ti, Hf g.b. segregation	2010
Molecular orbital	Ni	Y, Pt, S bonding	1985–1990
DFT	NiAl	RE, Pt, S bonding	2002–2018
ToF–SIMS	FeCrAl	Inward + outward growth	2017

However, conclusions equating *coincidence* as *primary cause and effect* may be misleading and less productive for further progress. For example, it is easy to observe the numerous RE effects, but overlook changes in sulfur interface segregation, since the latter often require specialized techniques. For undoped alloys, the indigenous low sulfur impurity levels of ~1–10 ppmw or more will almost certainly segregate, decrease interface strength, and lead to alumina scale spallation. Conversely, typical RE doping will almost certainly restrain sulfur segregation at typical impurity levels, thus preventing significant interfacial weakening, irrespective of, and simultaneously with, any other vestige or RE effect. Studies of scale spallation and adhesion mechanisms should address this conundrum or avoid it experimentally to allow for more robust conclusions.

The same is true of sulfur-based models that need to acknowledge secondary benefits of RE segregation and interfacial strengthening. The difficulty lies in quantifying each. In this regard, the stub pull test and the in-situ Auger scratch test provided a more definitive picture: the force required to remove the scale, the amount of scale removed, and correlations with underlying sulfur or RE interface segregation level (“[RE-S Counter-Doping and Critical Ratios](#)” section). Complementary cyclic oxidation behavior can be used to confirm those assessments. Non-adherent scales may not be retained well-enough to obtain meaningful results in a scratch or pull-off adhesion test; measurements of very high interfacial strength are limited by the epoxy strength. Characterizations can be supported by cross-sections using FIB-STEM EDS chemical information at nm level interfaces. Hydrogen charging or cathodic de-scaling potentials may offer an additional measure of adhesion strength.

Typical experimental designs may limit broader conclusions. Most successful low sulfur alloy studies focused on varying the sulfur content with no variation in the RE levels (Y, Hf in single crystal superalloys). On the other hand, most RE dopant studies relied on a fixed indigenous sulfur content, generally around 3–25 ppmw. While adherent behaviors were demonstrated with t_0 over 5000 h at 1100 °C and over 1000 h at 1150 °C for single crystal superalloys having just 6% Al, long term durability could not be sustained at 1200 °C. On the other hand, RE-doped NiAl, FeCrAl, and Fe–17Al alloys were shown to resist breakaway at 1150 °C, 1200 °C, and 1250 °C, respectively, for over 12,000 cycles (“[Comparison to Experimental Trends for Doped/Co-Doped Alloys](#)” section). Ni-base superalloys are distinguished by high temperature creep strength and load bearing applications, while the latter group consists of basically ductile heater alloys or brittle coating alloys with inadequate mechanical properties. The oxidation resistant wrought or ODS alloys generally possess both environmental and strength properties somewhere in between these two classes.

Note that in these comparative studies and in many of the recent cyclic life studies evaluating Al_2O_3 scales, 1000 h has become more of a standard demonstration of respectable life, with 5000–10,000 h tests in some cases. Temperatures of at least 1100 °C are a minimum requirement, with 1150° and 1200 °C becoming more common. It is no longer sufficient to present ≤ 100 h test results to discriminate and rank exceptional performance. In that regard, long-term, higher temperature performances of undoped, low sulfur NiCrAl, FeCrAl, and NiAl are not equivalent to

that of doped alloys. This may provide some differentiation between low S and RE-doped interfacial scale adhesion.

DFT has provided insights regarding Al_2O_3 -NiAl bond strengths (“[Theoretical Results](#)” section). Both the detrimental effect of S and improvements due to Hf, Zr, Y segregants are typically confirmed. Whether Hf and Zr are actually superior to Y dopants for alloys other than NiAl is a question raised by experimental evidence to the contrary. Thus, DFT of other FeCrAl, NiCrAl base systems (not just Ni or NiAl), closely compared to empirical results, may be instructive.

Other approaches relate to the segregation potential of sulfur. Sulfur activity in the alloy along with the surface energy decrease realized by interfacial segregation provide the thermodynamic driving forces based on sulfur content, the enthalpy of segregation, and alloy composition. The reactivity of sulfur-active RE dopants greatly affects sulfur activity. Reactivity may vary with free energy of their dopant-sulfides, while RE segregation is promoted by low solubility in the base alloy (e.g., for the series Sc, Ti, Y, Zr, La, Hf, Ce, Th). Alloy phases (γ -Ni-Al, γ' -Ni₃Al, and β -NiAl or NiCrAl vs FeCrAl vs superalloys) may provide additional insights. Experimental thermodynamic measurements would be welcome, but difficult. Thermodynamic modeling may be revealing, if databases exist.

Regarding RE co-doping, there are some interesting intersections across various phenomena. The systems seem to highlight combinations of tri-valent group RE_{III} and quadrivalent group RE_{IV}. For example, Y/Hf doped FeCrAl exhibited a cyclic oxidation performance peak of 12,500 h at 1200 °C (breakaway, Table 3 and Fig. 15). DFT modeling of Y/Hf doped Al_2O_3 -NiAl interfaces produced a 4× improvement in W_{ad} (“[Theoretical Results](#)” section). Permeability tests (“[Growth Stress](#)” section) of Lu_{III} and Hf_{IV} doped layered-wafers exhibited a 3× reduction in outer Al diffusivity (Hf) and a 2× reduction in inward O diffusivity (Lu). Furthermore, Y_{III}/Zr_{IV} co-doped bulk Al_2O_3 (“[Growth Stress](#)” section) enabled a 400× reduction in creep rate at 1250 °C and > 15× reduction observed for Nd_{III}/Zr_{IV} doping. The origins for such effects may appear disconnected: Oxidation effects (“[Atomistic Modeling Studies of Oxide-Metal Bonding](#)” and “[Comparison to Experimental Trends for Doped/Co-Doped Alloys](#)” sections) were related to Y/S and Hf/C gettering ratios. W_{ad} increases may simply arise from greater levels of total interfacial RE or specific interfacial arrangements. Creep effects may arise from special grain boundary complexions or electronic density of states that restrict electron/ionic defect transport. Some of these phenomena may just be coincidence, but others may imply a special RE_{III}/RE_{IV} synergy that influences bond strength.

Resolving outlier effects often has the serendipitous outcome of a novel or deeper level of overall understanding and new lines of development. Understanding exactly how Pt, with no sulfur reactivity, diminishes segregation and improves bond strength would be helpful. Initial DFT analyses have not found any bond enhancement for Pt-enriched interfaces but suggest a reduced sulfur diffusivity in a β -phase Ni-Pt-Al matrix. Careful studies identified unexpected Pt-Ni exchange at the interface and Pt reduction of sulfur transport in the base NiAl alloy (“[Pt Effects](#)” section). No other Pt-metal group element has been found to be particularly effective.

Detrimental effects of C, H, or H₂O on scale adhesion are sometimes indicated, but generally much less dominating than S; they may be of little practical

significance. But, in specific instances, it is useful to keep them in mind for perhaps making an adherent scale more so. Empirical verification of C (or H) at interfaces would be of interest, but difficult to analyze. SIMS and GDOES appear to be the most applicable techniques, but resolution limits for thick scales may be difficult.

In review, there is no lack of interesting avenues to explore. *Combining* techniques (below) across various base alloys may ultimately be more conclusive. Accordingly, some directions for evaluating, understanding, and improving scale adhesion (cyclic oxidation resistance) are offered:

Experimental:

Experimental bond strength (tensile or scratch test) vs RE dopant, S content, and interfacial segregation levels for various base alloys.

Adhesion or failure correlations with diffusional and mechanical (creep) properties of the scale and alloy.

Modeling:

Sulfur thermodynamic activity in the substrate vs dopant level, reactivity, and solubility, as well as base alloy composition. Interface energetics for site competition (Pt, RE) or co-segregation (Cr) vs S.

DFT of bond strength for various dopant and sulfur levels, applied to various base alloys. The possibility of H and C effects could also be considered.

Summary and Concluding Remarks

This chronological assessment attempted to retrace advances in understanding protective Al_2O_3 scale adhesion for typical oxidation-resistant, high-temperature alloys. The classic mechanisms were addressed: pegging, scale plasticity, growth stress, and vacancy sink. Historical evidence was cited that conclusively contradicted each of these proposed mechanisms. Subsequently, most empirical results and current understanding (since 1985) support the chemical bond theory. Herein scale spallation from undoped alloys is triggered by bond weakening resulting from strong (>20%) sulfur (impurity) segregation, from only a few ppm in the base alloy. Removing sulfur to 0.1 ppmw levels in the bulk alloy precludes segregation and can produce excellent cyclic oxidation resistance, without reactive elements. Sulfur reductions also eliminate detrimental void production. Sulfur-reactive (\approx oxygen-reactive) RE element doping at ~ 0.01 – 0.1% levels produce adherent scales primarily by reducing sulfur activity and segregation. This may occur in solution or by forming complexes or precipitates. Additional adhesive strength can be conferred by reactive element interfacial segregation, but cannot totally counteract intentionally sulfur-doped alloys (e.g., where $S \geq \text{RE}$). Other reactive element effects may be beneficial in secondary roles (reducing carbon and moisture-induced spallation effects, decreasing grain boundary diffusion (growth) and creep (deformation) in the scale or base alloy).

Quantifying the contributions of each RE effect in a balanced fashion has been challenging. Combining diverse techniques over a variety of base alloys may improve understanding, but with the cost of experimental complexity. DFT models of interfacial strength offer more flexibility, but current results do not closely rank RE dopant effects on strength according to experimental cyclic oxidation weight change results. RE_{III} and RE_{IV} co-doping suggest intriguing intersections among phenomena: outstanding cyclic oxidation life, DFT interface strength, and, respectively, reduced O and Al grain boundary diffusivity, as well as S and C interactions in the base metal. Thermodynamic assessments of S-RE-base metal interactions may provide additional understanding of segregation potential and consequent scale adhesion. Given the immense body of prior work associated with scale adhesion, advanced literature search algorithms may uncover details of countless pertinent past studies in order to optimize new studies.

Appendix: Summary of Point-by-Point Logic Assessments

1. Pegging

Premise: RE-doped alloys form adherent scales because RE-oxide intrusions impart interlocking mechanical strength to the interface.

Contradiction: Many RE-doped alloys form adherent scales without pegs. Low sulfur alumina-forming superalloys form very durable scales without RE or pegs. There may be instances of spallation of RE/S co-doped alloys, with pegs.

- Pegs are **not necessary or sufficient** for adhesion.

2. Scale Plasticity

Premise: RE-doped alloys form adherent scales because the scale is generally finer grain size with more opportunity for stress relief by grain boundary deformation processes.

Contradiction: RE-doped bulk aluminas are orders of magnitude *more* creep resistant than pure or Ti-doped Al₂O₃. RE grain boundary segregation is universally found, reduces grain boundary diffusivity and Coble creep. Plasticity is actually more prevalent for undoped scales, which indeed wrinkle at temperature and delaminate upon cooling.

- Scale plasticity is **neither sufficient nor necessary** to produce adhesion. In fact, greater plasticity is associated with non-adherent behavior.

3. Growth stress

Premise: RE-doped alloys form columnar adherent scales because growth is primarily by stress-free oxygen inward diffusion and preferential growth at the metal interface. Equiaxed scales for undoped alloys results from both outward Al and inward O diffusion. This allows growth within the scale and produces highly stressed, convoluted scales and spallation.

Contradiction: Growth stresses were calculated from residual stress actually measured by photo-luminescence spectroscopy. The stress on adherent scales for RE-doped alloys (-1 GPa) was greater than that determined for non-adherent scales on undoped alloys. Convolutions occur because of Coble creep and debonding of undoped Al_2O_3 scales. RE doped scales are more resistant to creep and buckling, but still under high stress. Changes in growth direction and reduced kinetics do not dominate adhesion. Increased growth stress does not independently cause spallation, though it may contribute to long term strain energy and eventual breakaway failure of adherent scales.

- Decreased growth stress is **not sufficient or necessary** to produce adhesion.

4. Vacancy Sink

Premise: Interfacial porosity destroys large areas of scale-metal attachment, allowing debonding, stress concentrations, and spallation upon cooling. Outward Al growth produces interfacial vacancies that form voids on undoped alloys. RE-doped or oxide-dispersed alloys provide numerous internal sites for vacancy annihilation.

Contradiction: Interfacial scale spallation has been observed without voids. Some outward growth occurs on RE-doped alloys without void formation. Al_2O_3 dispersoids are not sufficient to prevent void formation and produce adherent scales, only RE dispersoids are. Sulfur doping can exacerbate void formation, even with RE-doping. Desulfurizing can eliminate void production and impart adhesion without dispersoids or RE doping.

- Voids are **not necessary** for spallation. Outward growth is **not sufficient** to produce voids. RE-doping is **not sufficient** to prevent voids. Vacancy sinks are **neither sufficient nor necessary** for adhesion.

5. Graded Seal

Premise: An interlayer forms with a chemical gradient that ‘spreads’ the thermal expansion mismatch stress and diffuses any interfacial stress concentration.

Contradiction: FIB-STEM cross-sections of adherent Al_2O_3 scales on RE-doped substrates show no discreet, graded interfacial layer. Interfacial chemical segregation has been observed, but only over 1–2 nm. A CTE gradient across the entire μm 's- thick scale would only displace the highest stress, not eliminate it.

- No graded interfacial scale phase is observed for adherent scales; a graded seal is **not necessary or sufficient** for adhesion.

6. Chemical Bond

Premise 5a: RE elements segregate to the oxide-metal interface and produce a strong interfacial chemical bond that prevents spallation.

Partial Contradiction: Scale adhesion can be produced for low sulfur alloys without RE. Single crystal superalloys with Hf do not necessarily form fully adherent scales. Adding enough sulfur to RE-doped alloys destroys scale adhesion.

- RE-doping is **not always necessary** for (primary) adhesion. RE-doping is **not always sufficient** for (primary) adhesion.

Premise 5b: Sulfur removal precludes sulfur segregation and bond weakening. RE element dopants also prevent indigenous ppm sulfur impurities from interface segregation and bond weakening. Sulfur co-doping with RE prevents an adherent scale, except for high RE/S levels or at very low ppm levels of S.

Partial Contradiction: RE-dopants may also segregate and strengthen the interfacial bond for low sulfur alloys.

- Sulfur removal is **sufficient** to produce (primary) scale adhesion for undoped alloys. Sulfur doping RE-doped alloys is **sufficient** to produce spallation. Further (secondary) strengthening by RE-doping may occur, but **may not be necessary**. Control of sulfur segregation is always **necessary** for adhesion.

Secondary factors. Carbon may be a detrimental contaminant but much less powerful compared to sulfur. In that regard, Hf-C interactions are helpful, but Hf doping in single crystal superalloys does not preclude some spallation. Also, moisture removes partially adherent scales on alloys having intermediate sulfur levels and may contribute to delayed spallation of highly stressed more adherent scales. Electrochemical hydrogen charging can strip an adherent scale on RE-doped superalloys. Pt improves scale adhesion, especially on β -NiAl, but in large part by somehow curtailing sulfur segregation.

- C, H₂O (H) may be secondary factors increasing spallation, presumably by interfacial segregation, but are **not necessary**. Pt is helpful in reducing sulfur segregation and increasing adhesion, especially for NiAl, but is **not necessary**.

Acknowledgements This overview perspective was enabled by 50 years of involvement with advanced high temperature aero-turbine materials supported at the NASA Glenn (nee Lewis) Research Center. The cyclic oxidation legacies of NASA researchers (C. Lowell, C. Barrett, R. Garlick, J. Doychak, J. Nesbitt, and many more) are gratefully acknowledged. The author is grateful for information provided by K. Unocic, V. Tolpygo, B. Pint, D. Monceau, R. Swadźba, K. Harris, and to P. Tortorelli for reviewing the manuscript. Associations, communications, and collaborations with many of the referenced authors and Advisory Boards, have been invaluable.

References

1. D. G. Lees, *Oxidation of Metals* **27**, 75 (1987). <https://doi.org/10.1007/BF00656731>.
2. D. G. Lees, *Proceedings of the Royal Society of London Series A* **459**, 1459 (2003).
3. B. A. Pint, *Oxidation of Metals* **45**, 1 (1996). <https://doi.org/10.1007/BF01046818>.
4. D. P. Whittle and J. Stringer, *Philosophical Transactions of the Royal Society of London Series A* **295**, 309 (1980). <https://doi.org/10.1098/rsta.1980.0124>.
5. H. Hindam and D. P. Whittle, *Oxidation of Metals* **18**, 245 (1982). <https://doi.org/10.1007/BF00656571>.
6. J. L. Smialek and R. Browning, Current Viewpoints on Oxide Adherence Mechanisms. NASA TM-87143, October 1985, (also, Electrochem. Soc. Symp. Proc. on High Temp. Matls. Chem. III, eds. Z. A. Munir and D. Cubicciotti, 1986: 259–271).
7. *The Reactive Element Effect on High Temperature Oxidation-After Fifty Years*, edited by W.E. King (Materials Science Forum 43, Trans. Tech Publications, Switzerland, 1989).
8. *The Role of Active Elements in the Oxidation Behaviour of High Temperature Metals and Alloys*. E. Lang, ed., CEC Joint Research Centre, Institute of Advanced Materials, Petten, The Netherlands. (Elsevier, London, 1989). <https://doi.org/10.1007/978-94-009-1147-5>.
9. F. H. Stott, G. C. Wood, and J. Stringer, *Oxidation of Metals* **44**, 113 (1995). <https://doi.org/10.1007/BF01046725>.
10. B. A. Pint, in *Proceedings of John Stringer Symposium on High Temperature Corrosion*, eds. P. F. Tortorelli, I. G. Wright, and P. Y. Hou (ASM International, Materials Park, OH, 2003), p. 9–19.
11. P. Y. Hou, *Materials Science Forum*. **696**, 39 (2011). <https://doi.org/10.4028/www.scientific.net/MSF.696.39>.
12. D. Naumenko, B. A. Pint, and W. J. Quadackers, *Oxidation of Metals* **86**, 1 (2016). <https://doi.org/10.1007/s11085-016-9625-0>.
13. B. A. Pint, High Temperature Corrosion of Alumina-forming Iron, Nickel and Cobalt-base Alloys, in *Shreir's Corrosion, Fourth Edition*. 2010, p. 606–645.

14. J. K. Tien and F. S. Pettit, *Metallurgical and Materials Transactions* **3**, 1587 (1972). <https://doi.org/10.1007/BF02643050>.
15. F. A. Golightly, F. H. Stott, and G. C. Wood, *Oxidation of Metals* **10**, 163 (1976).
16. A. M. Huntz, Effect of Active Elements on the Oxidation Behaviour of Al_2O_3 -Formers, in *The Role of Active Elements in the Oxidation Behaviour of High Temperature Metals and Alloys*, ed. E. Lang. CEC Joint Research Centre, Institute of Advanced Materials, Petten, The Netherlands. (Elsevier, London, 1989). <https://doi.org/10.1007/978-94-009-1147-5>.
17. J. D. Kuenzly and D. L. Douglass, *Oxidation of Metals* **8**, 139 (1974). <https://doi.org/10.1007/BF00612170>.
18. A. Kumar, M. Nasrallah, and D. L. Douglass, *Oxidation of Metals* **8**, 227 (1974). <https://doi.org/10.1007/BF00604042>.
19. C. Giggins and F. S. Pettit, Oxide Scale Adherence Mechanisms and the Effects of Yttrium, Oxide Particles and Externally Applied Loads on the Oxidation of NiCrAl and CoCrAl Alloys. ARL 75-0234, (1975), Contract FF 33615-72-6-1702 Final Report, WPAFB, OH.
20. J. G. Smeggil, A. W. Funkenbush, and N. S. Bornstein, The Electrochemical Society Extended Abstracts, no. 21. 1984;84–1:27. (Cincinnati, OH, May 6–11, 1984).
21. D. Naumenko, B. Gleeson, E. Wessel, L. Singheiser, and W. J. Quadackers, *Metallurgical and Materials Transactions A* **38A**, 2974 (2007).
22. K. Unocic, private communication, ORNL, 2017.
23. V. Tolpygo, private communication, also presented at HTCPM-7 (2008), les Embiez.
24. J. L. Smialek and G. H. Meier, in *Superalloys II*, eds. C. T. Sims, N. S. Stoloff, and W. C. Hagel (Wiley & Sons, NY, 1987), p. 293–326.
25. J. L. Smialek, N. S. Jacobson, B. Gleeson, D. B. Hovis, and A. H. Heuer, *Oxygen Permeability and Grain-Boundary Diffusion Applied to Alumina Scales*. NASA/TM—2013-217855, Aug. 2013. NASA Technical Reports Server (NTRS).
26. D. L. Deadmore and C. E. Lowell, *Oxidation of Metals* **11**, 91 (1977).
27. R. Swadźba, L. Swadźba, J. Wiedermann, et al., *Oxidation of Metals* **82**, 195 (2014). <https://doi.org/10.1007/s11085-014-9487-2>.
28. J. G. Smeggil, A. W. Funkenbusch, and N. S. Bornstein, *Metallurgical and Materials Transactions* **17**, 923 (1986). <https://doi.org/10.1007/BF02661258>.
29. K. L. Luthra and C. L. Briant, *Oxidation of Metals* **26**, 397 (1986). <https://doi.org/10.1007/BF00659344>.
30. K. Przybylski, A. J. Garratt-Reed, B. A. Pint, E. P. Katz, and G. J. Yurek, *Journal of The Electrochemical Society* **134**, 3208 (1987).
31. B. A. Pint, A. J. Garratt-Reed, and L. W. Hobbs, *Materials at High Temperatures* **13**, 3 (1995).
32. C. Mennicke, E. Schumann, M. Ruhle, et al., *Oxidation of Metals*. **49**, 455 (1998). <https://doi.org/10.1023/A:1018803113093>.
33. K. A. Unocic and B. A. Pint, *Surface & Coatings Technology* **205**, 1178 (2010).
34. M. A. Gölgün, R. Voytovych, I. Maclaren, and R. M. Ruhle, *Interface Science* **10**, 99 (2002). <https://doi.org/10.1023/A:1015268232315>.
35. Y. Z. Li, C. Wang, H. M. Chan, J. M. Rickman, and M. P. Harmer, *Journal of the American Ceramic Society* **82**, 1497 (1999).
36. V. K. Tolpygo and D. R. Clarke, *Acta Materialia* **46**, 5153 (1998). [https://doi.org/10.1016/S1359-6454\(98\)00133-5](https://doi.org/10.1016/S1359-6454(98)00133-5).
37. V. K. Tolpygo and D. R. Clarke, *Oxidation of Metals* **49**, 187 (1998). <https://doi.org/10.1023/A:101882861902810.1007/BF01046985>.
38. D. M. Lipkin and D. R. Clarke, *Oxidation of Metals* **45**, 267 (1996).
39. D. Renusch, M. Grimsditch, I. Koshelev, B. W. Veal, and P. Y. Hou, *Oxidation of Metals* **48**, 471 (1997).
40. V. K. Tolpygo, J. R. Dryden, and D. R. Clarke, *Acta Materialia* **46**, 927 (1998). [https://doi.org/10.1016/S1359-6454\(97\)00306-6](https://doi.org/10.1016/S1359-6454(97)00306-6).
41. C. Mennicke, D. R. Clarke, and M. Rühle, *Oxidation of Metals* **55**, 551 (2001).
42. M. C. Stasik, F. S. Pettit, G. H. Meier, A. Ashary, and J. L. Smialek, *Scripta Metallurgica et Materialia* **31**, 1645 (1994).
43. G. H. Meier, F. S. Pettit, and J. L. Smialek, *Materials and Corrosion* **46**, 232 (1995). <https://doi.org/10.1002/maco.19950460407>.
44. J. Cho, C. Wang, H. M. Chan, J. M. Rickman, and M. P. Harmer, *Acta Materialia* **47**, 4197 (1999).


45. J. Cho, C. Wang, H. M. Chan, J. M. Rickman, and M. P. Harmer, *Journal of Materials Research* **16**, 425 (2000).
46. C. M. Wang, J. Cho, H. M. Chan, M. P. Harmer, and J. M. Rickman, *Journal of the American Ceramic Society* **84**, 1010 (2001). <https://doi.org/10.1111/j.1151-2916.2001.tb00783.x>.
47. S. Yasuda, H. Yoshida, T. Yamamoto, and T. Sakuma, *Materials Transaction* **45**, 2078 (2004). <https://doi.org/10.2320/matertrans.45.2078>.
48. V. K. Tolpygo and D. R. Clarke, *Materials at High Temperatures* **20**, 261 (2003). <https://doi.org/10.1179/mht.2003.030>.
49. J. A. Nychka and D. R. Clarke, *Oxidation of Metals* **63**, 325 (2005). <https://doi.org/10.1007/s11085-005-4391-4>.
50. H. M. Hindam and W. W. Smeltzer, *Journal of the Electrochemical Society* **127**, 1622 (1980).
51. G. C. Rybicki and J. L. Smialek, *Oxidation of Metals* **31**, 275 (1989).
52. E. J. Felten and F. S. Pettit, *Oxidation of Metals* **10**, 189 (1976). <https://doi.org/10.1007/BF00612159>.
53. K. P. R. Reddy, J. L. Smialek, and A. R. Cooper, *Oxidation of Metals* **17**, 429 (1982). <https://doi.org/10.1007/BF00742122>.
54. R. Prescott and M. J. Graham, *Oxidation of Metals* **38**, 233 (1992). <https://doi.org/10.1007/BF00666913>.
55. K. Abbasi, M. Zahiri, and A. H. Heuer, *Materials Performance and Characterization*. **6**, 292 (2017). <https://doi.org/10.1520/MPC20160063>.
56. T. Matsudaira, M. Wada, T. Saitoh, and K. Kitaoka, *Acta Materialia* **58**, 1544 (2010).
57. T. Matsudaira, M. Wada, T. Saitoh, and K. Kitaoka, *Acta Materialia* **59**, 5440 (2011).
58. S. Kitaoka, T. Matsudaira, M. Wada, T. Saitoh, M. Tanaka, and Y. Kagawa, *Journal of the American Ceramic Society* **97**, 2314 (2014). <https://doi.org/10.1111/jace.12935>.
59. T. Huang, D. Naumenko, P. Song, J. Lu, and W. J. Quadackers, *Oxidation of Metals* **90**, 671 (2018).
60. A. H. Heuer, et al., *Acta Materialia* **61**, 6670 (2013).
61. A. W. Funkenbusch, J. G. Smeggil, and N. S. Bornstein, *Metallurgical and Materials Transactions A* **16**, 1164 (1985). <https://doi.org/10.1007/BF02811687>.
62. K. C. Mills, *Thermodynamic Data for Inorganic Sulfides, Selenides and Tellurides*. JANAF Tables, (Butterworth, 1974).
63. I. Barin and O. Knacke, *Thermochemical Properties of Inorganic Substances*, (Springer, 1977).
64. D. R. Sigler, *Oxidation of Metals* **32**, 337 (1989).
65. C. L. Briant and K. L. Luthra, *Metallurgical and Materials Transactions A* **19**, 2099 (1988). <https://doi.org/10.1007/BF02645212>.
66. P. Y. Hou, *Annual Review of Materials Research* **38**, 275 (2008).
67. D. T. Jayne and J. L. Smialek, in *Microscopy of Oxidation II*, eds. S. B. Newcomb and M. J. Bennett (Institute of Metals, 1993), p. 183–196 (also NASA TM 106289, 1993).
68. P. Fox, D. G. Lees, and G. W. Lorimer, *Oxidation of Metals* **36**, 491 (1991). <https://doi.org/10.1007/BF01151594>.
69. K. Prußner, E. Schumann, and M. Rühle, in *Fundamental Aspects of High Temperature Corrosion*, eds. D. A. Shores, R. A. Rapp, and P. Y. Hou (The Electrochem. Soc. 1996), p. 344.
70. P. Y. Hou and J. Stringer, *Oxidation of Metals* **38**, 323 (1992). <https://doi.org/10.1007/BF00665658>.
71. P. Y. Hou and K. Priimak, *Oxidation of Metals* **63**, 113 (2005).
72. P. Y. Hou, *Materials Science Forum* **696**, 39 (2011).
73. M. Bai, H. Jiang, Y. Chen, Y. Chen, C. Grovenor, X. Zhao, and P. Xiao, *Materials and Design* **97**, 364 (2016).
74. H. J. Grabke, D. Wiemer, and H. Viehhaus, *Applied Surface Science* **47**, 243 (1991).
75. D. Wiemer, H. J. Grabke, and H. Viehhaus, *Fresenius Journal of Analytical Chemistry* **341**, 402 (1991). <https://doi.org/10.1007/BF00321944>.
76. C. Tabata, K. Kawagishi, J. Uzuhashi, T. Ohkubo, K. Hono, T. Yokokawa, H. Harada, and S. Suzuki, *Scripta Materialia* **194**, 113616 (2021). <https://doi.org/10.1016/j.scriptamat.2020.11.003>.
77. R. Tran, Z. Xu, B. Radhakrishnan, D. Winston, W. Sun, K. A. Persson, and S. P. Ong, *Scientific Data* **3**, 160080 (2016). <https://doi.org/10.1038/sdata.2016.80>.
78. P. D. Tapesch and A. A. Quong, *Physica Status Solidi B* **217**, 377 (2000). [https://doi.org/10.1002/\(SICI\)1521-3951\(200001\)217:1%3c377::AID-PSSB377%3e3.0.CO;2-B](https://doi.org/10.1002/(SICI)1521-3951(200001)217:1%3c377::AID-PSSB377%3e3.0.CO;2-B).
79. B. A. Pint and L. W. Hobbs, *Journal of The Electrochemical Society* **141**, 2443 (1994).

80. A. S. Khanna, C. Wasserfuhr, W. J. Quadackers, and H. Nickel, *Materials Science and Engineering: A* **120–121**, 185 (1989).
81. J. L. Smialek, in *Proceedings of High Temperature Materials Chemistry IV*, eds. Z. A. Munir, D. Cubicciotti, and H. Tagawa (Electrochem. Soc., 1988), p. 241–253 (also NASA TM 100209, 1987).
82. J. L. Smialek and B. A. Pint, Optimizing Scale Adhesion for Single Crystal Superalloys. *Materials Science Forum, HTCPM-5*. (2001;369–372, 459–466). (also NASA TM 2000-210362).
83. W. Wang, D. Li, J. Chang, H. Guo, S. Gong, and H. Xu, *Journal of Materials Science and Technology* **30**, 229 (2014).
84. P. Y. Hou, *Oxidation of Metals*. **52**, 337 (1999).
85. J. G. Smeggil, N. S. Bornstein, and M. A. DeCrescente, *Oxidation of Metals* **30**, 259 (1988). <https://doi.org/10.1007/BF00666602>.
86. J. L. Smialek, Adherent Al₂O₃ Scales Formed on Undoped NiCrAl Alloys. *N. L. Peterson Memorial Symposium Proceedings on Oxidation and Associated Mass Transport, TMS-AIME* (1986;Oct), p. 297–313.
87. J. L. Smialek, *Metallurgical Transactions A Communication* **18**, 164 (1987).
88. M. A. DeCrescente, N. S. Bornstein, and J. G. Smeggil, Oxidation Resistant Superalloys Containing Low Sulfur Levels. US Patent 4895201. 1990;Jan 23:1–9.
89. J. L. Smialek, *Metallurgical Transactions A* **22**, 739 (1991).
90. J. L. Smialek and B. K. Tubbs, Effect of Sulfur Removal on Scale Adhesion to PWA 1480. *Metallurgical and Materials Transactions A*. **26**, 427 (1995). (also in *Corrosion and Particle Erosion at High Temperatures*, V. Srinivasan, K. Vedula, eds., TMS-AIME, 1989, 459–487).
91. R. Janakiraman, G. H. Meier, and F. S. Pettit, *Metallurgical and Materials Transactions A*. **30**, 2905 (1999).
92. J. S. Smialek, D. T. Jayne, J. C. Schaeffer, and W. C. Murphy, *Thin Solid Films* **253**, 285 (1994). Also NASA TM 106734, 1994. <https://ntrs.nasa.gov/citations/19950007254>.
93. J. L. Smialek, Oxidation Resistance and Critical Sulfur Content of Single Crystal Superalloys. Presented at the *Congress of the International Gas Turbine Institute*, Birmingham, UK, 1996, Paper ASME 96-GT-519, 7 pages; also *J. Engineering for Gas Turbines and Power, ASME Transactions*. 1998;120:370–374.
94. J. L. Smialek, *Crystals* **11**, 60 (2021). <https://doi.org/10.3390/cryst11010060>.
95. P. Audigé, A. Rouaix-Vande Put, A. Malié, and D. Monceau, *Corrosion Science* **144**, 127 (2018).
96. E. J. Felten, *Oxidation of Metals* **10**, 23 (1976). <https://doi.org/10.1007/BF00611696>.
97. E. C. Dickey, B. A. Pint, K. B. Alexander, and I. G. Wright, *Journal of Materials Research* **14**, 4531 (1999). <https://doi.org/10.1557/JMR.1999.0615>.
98. B. A. Pint, I. G. Wright, W. Y. Lee, Y. Zhang, K. Prüßner, and K. B. Alexander, *Materials Science and Engineering A* **245**, 201 (1998). [https://doi.org/10.1016/S0921-5093\(97\)00851-4](https://doi.org/10.1016/S0921-5093(97)00851-4).
99. K. Murphy, Pt–Al–Hf/Zr Coating and Method. U.S. Patent Application Pub. No. US2010/0297471 A1. Nov. 25, 2010.
100. B. Gleeson, N. Mu, and S. Hayashi, *Journal of Material Science* **44**, 1704 (2009). <https://doi.org/10.1007/s10853-009-3251-z>.
101. P. Y. Hou and V. K. Tolpygo, Examination of the platinum effect on the oxidation behavior of nickel-aluminide coatings. in *Coatings for Use at High Temperature, International Conference on Metallurgical Coatings and Thin Films (ICMC-TF)*, AVS, San Diego, April 23–27, 2007. Also, *Surface and Coatings Technology*, **202**, 623 (2007).
102. I. Szymerska and M. Lipski, *Journal of Catalysis* **47**, 144 (1977).
103. T. Gheno, D. Monceau, D. Ouqab, and Y. Cadoret, *Oxidation of Metals* **73**, 95 (2009). <https://doi.org/10.1007/s11085-009-9164-z>.
104. J. Ramé, et al, in *Superalloys 2020*, eds. S. Tin et al. The Minerals, Metals & Materials Series. (Springer, Cham. 2020), p. 71–81 <https://doi.org/10.1007/978-3-030-51834-9>.
105. J. L. Smialek, *JOM* **1**, 29 (2006). (Condensed from NASA TM 2005-214030). <https://ntrs.nasa.gov/api/citations/20060004789/downloads/20060004789.pdf>.
106. B. A. Pint, J. A. Haynes, Y. Zhang, K. More, and I. G. Wright, *Surface and Coatings Technology* **201**, 3852 (2006).
107. A. K. Kuruvilla and N. S. Stoloff, *Scripta Metallurgica* **19**, 83 (1985).
108. J. L. Smialek, Moisture-Induced Alumina Scale Spallation: The Hydrogen Factor. NASA/TM-2010-216260, April, 2010. 31 pages. <http://ntrs.nasa.gov/search.jsp?R=20100021167>.

109. J. L. Smialek, *Surface and Coatings Technology* **206**, 1577 (2011). <https://doi.org/10.1016/j.surfcoat.2011.07.015>.
110. G. Hultquist, M. J. Graham, J. L. Smialek, and B. Jönsson, *Corrosion Science* **93**, 324 (2015).
111. K. H. Johnson and S. V. Pepper, *Journal of Applied Physics* **53**, 6634 (1982).
112. A. B. Anderson, S. D. Mehendru, and J. L. Smialek, *Journal of the Electrochemical Society* **132**, 1695 (1985).
113. S. Y. Hong, A. B. Anderson, and J. L. Smialek, *Surface Science* **230**, 174 (1990).
114. E. A. Jarvis and E. A. Carter, *Computing in Science & Engineering*. **March/April**, 33 (2002).
115. K. M. Carling and E. A. Carter, *Acta Materialia* **55**, 2791 (2007). <https://doi.org/10.1016/j.actamat.2006.12.020>.
116. W. Zhang, J. R. Smith, X. G. Wang, and A. G. Evans, *Physical Review B* **67**, 245414 (2003). <https://doi.org/10.1063/1.2907339>.
117. Y. Jiang, J. R. Smith, and A. G. Evans, *Applied Physics Letters* **92**, 141918 (2008). <https://doi.org/10.1063/1.2907339>.
118. X. G. Wang and J. R. Smith, *Physical Review B* **70**, 081401(R) (2004).
119. I. Ozfidan, K. Chen, and M. Fu, *Metallurgical and Materials Transactions A* **42**, 4126 (2011). <https://doi.org/10.1007/s11661-011-0813-x>.
120. A. B. Anderson, C. Ravimohan, and S. P. Mehendru, *Surface Science* **183**, 438 (1987).
121. F. Christien, P. Pouteau, R. Le Gall, G. Saindrenan, and Y. Jaslier, *Journal de Physique IV France* **10**, 173 (2000). <https://doi.org/10.1051/jp4:2000424>.
122. K. Chen, *Journal of Physics D: Applied Physics* **49**, 055306 (2016).
123. R. F. Zhang, D. Zhang, D. Q. Legut, S. H. Li, Z. H. Zhang, H. Fu, and H. B. Guo, *Physical Chemistry Chemical Physics* **18**, 22864 (2016).
124. J. Bennett, J. M. Kranenburg, and W. G. Sloof, *Journal of the American Ceramic Society* **88**, 2209 (2005). <https://doi.org/10.1111/j.1551-2916.2005.00408.x>.
125. J. Bennett and W. G. Sloof, *Materials and Corrosion* **57**, 223 (2006). <https://doi.org/10.1002/maco.200503928>.
126. B. A. Pint, *Journal of the American Ceramic Society* **86**, 686 (2003). <https://doi.org/10.1111/j.1151-2916.2003.tb03358.x>.
127. H. Guo, D. Li, L. Zheng, S. Gong, and H. Xu, *Corrosion Science* **88**, 197 (2014).
128. T. Gheno, B. C. Zhou, A. Ross, et al., *Oxidation of Metals* **87**, 297 (2017). <https://doi.org/10.1007/s11085-016-9706-0>.
129. T. J. Tallman, B. Anasori, and M. W. Barsoum, *Materials Research Letters* **1**, 115 (2013). <https://doi.org/10.1080/21663831.2013.806364>.
130. J. L. Smialek, *Corrosion Science* **91**, 281 (2015).
131. J. W. Byeon, J. Liu, M. Hopkins, W. Fischer, N. Garimella, K. B. Park, M. P. Brady, M. Radovic, T. El-Raghy, and Y. H. Sohn, *Oxidation of Metals* **68**, 97 (2007). <https://doi.org/10.1007/s11085-007-9063-0>.
132. J. L. Smialek, B. J. Harder, and A. Garg, *Surface and Coatings Technology* **285**, 77 (2016). <https://doi.org/10.1016/j.surfcoat.2015.11.018>.
133. X. Li, Y. Qian, L. Zheng, J. Xu, and M. Li, *Journal of the European Ceramic Society* **36**, 3311 (2016).
134. J. L. Smialek, Unusual Oxidative Limitations for Al-MAX Phases. NASA/TM-2017-219444, February, 2017, 30 pages.
135. S. Badie, D. Sebold, R. Vaßen, O. Guillon, and J. Gonzalez-Julian, *Acta Materialia* **215**, 117025 (2021). <https://doi.org/10.1016/j.actamat.2021.117025>.
136. D. B. Lee and T. D. Nguyen, *Journal of Alloys and Compounds* **464**, 434 (2008).

Publisher's Note Springer Nature remains neutral with regard to jurisdictional claims in published maps and institutional affiliations.

Authors and Affiliations

James L. Smialek¹ 

✉ James L. Smialek
Dr.JSmialek@Outlook.com

¹ NASA Glenn Research Center, (retired), Strongsville, OH 44149, USA